THE UNIVERSITY OF MANITOBA

ANALYSIS OF A MICROWAVE VOID FRACTION MONITOR

by

JOHN H. BOYACHOK

A THESIS

SUBMITTED TO THE FACULTY OF GRADUATE STUDIES

IN PARTIAL FULFILMENT OF THE REQUIREMENTS FOR THE DEGREE

OF MASTER OF SCIENCE IN ENGINEERING

DEPARTMENT of ELECTRICAL ENGINEERING

WINNIPEG, MANITOBA

OCTOBER, 1974.

ANALYSIS OF A MICROWAVE VOID FRACTION MONITOR

by

JOHN H. BOYACHOK

A dissertation submitted to the Faculty of Graduate Studies of the University of Manitoba in partial fulfillment of the requirements of the degree of

MASTER OF SCIENCE

ACKNOWLEDGEMENTS

I wish to thank Dr. M.A.K. Hamid for his assistance in formulating the problem and for supervising the research work. I also wish to thank Dr. S.J. Towaij and Dr. P. Bhartia for aiding me with the mathematical and numerical aspects of the computations. The able typing of both Miss Janet Gourlay and Mrs. Ann Craig is heartily appreciated. I would also like to thank Mr. Walter Stachuk of the Ministry of Transport for his assistance in getting the thesis prepared. Finally, the financial assistance of the Atomic Energy of Canada Limited, through a research grant and the National Research Council, grant A-3326 are gratefully acknowledged.

ABSTRACT

The eigenvalue problem of an open-ended, dielectric loaded, circular cylindrical resonator is investigated by the boundary value and numerical techniques to compute the volumetric void fraction of gas bubbles in organic oil coolants used in some modern nuclear reactors. The resonator sensing section geometry is such that an organic coolant (or similar material) is transported through circular pipes acting as waveguides on both sides of the resonator section whose diameter is enlarged by a dielectric ring. The results are shown to be in excellent agreement with experimental data for the special case when the dielectric in the enlargement is the same as the transported material.

The technique is based on the perturbation method and leads to a linear shift in the resonant frequency of the sensor with a linear change in the void fraction. It is also shown that when the relative permittivity of the dielectric material in the ring exceeds that of the transported material, the Q-factor of the resonator rises at the expense of over-moding where higher order modes may be excited and resonated within the narrower bandwidth of the desired sensing mode. An examination of the requirements for optimum sensitivity is done from the computed data and it is shown that the best sensitivity is achieved when the annular ring and the coolant have the same permittivity.

TABLE OF CONTENTS

1. INTRODUCTION

1.1. General

Since 1941, when Enrico Fermi first was able to control the fission process of atomic particles, there have been many advances made in the design of nuclear reactors. Similar advances have been made in the study of materials necessary to the construction and operation of these reactors. A number of researchers have investigated the properties of fluid materials for use as reactor moderators and/or coolants. Materials that have been investigated include heavy and light water, liquid metals, various gases and organic materials. Though the use of organic materials in this capacity was first suggested in the United States during the Manhattan Project of the Second World War, it was not until the early years of the 1950's that the necessary technology and techniques were acquired to allow for the establishment of the first test reactor using organic materials.

The first experimental reactor using this material was the Organic Moderated Reactor Experiment (OMRE) established in 1953 by the American Atomic Energy Commission. Tests conducted with this reactor confirmed many of the foreseen advantages and disadvantages of organic materials(1). The advantages included the low vapour pressure of the organic, the non-corrosiveness of the material to the structural hardware (eg. pipes, valves) of the reactor, and the small amount of induced radioactivity in the organic material caused by the bombardment of neutron particles. The most serious disadvantage encountered was the partial decomposition of the organic material into higher molecular weight polymers and lower molecular weight gases chiefly nitrogen. This decomposition occurred when the material, at the operating temperature of over 300°C, was bombarded by the nuclear particles. The resulting polymers were deposited out of the organic material onto metal surfaces where they fouled the piping, fuel elements, and cooling areas. The gases remained in the coolant but were found to increase the corrosiveness and decrease the desired cooling properties of the organic.

While the above-mentioned products of decomposition could readily be removed from the organic coolant, no techniques were available to determine the concentrations of these materials aside from subjecting a sample of the coolant to chemical tests. Accurate and immediate knowledge of the concentrations would allow corrective measures to be taken and greatly enhance the value of the reactor as an experimental tool. A practical method of monitoring the rate of decomposition would therefore have to provide continuous on-line data without disturbing the flow of the coolant.

As the organic coolant and the products of the decomposition process are dielectric materials of various dielectric constants, it is reasonable to assume that different concentrations of these materials will have different dielectric constants. It is therefore suggested that measurement of the dielectric constant of the mixture would provide information as to the amount of decomposition.

While there are many methods of determining the dielectric constant of a material or a mixture of materials (for example, impedance bridges at low frequencies, resonant cavities and circuits at high frequencies) none of these are suitable under the physical conditions that are present while the reactor is operating. Typical values of temperature and pressure of the coolant are $400^{\circ}C$ and 400 psi respectively. Also, the condition was imposed that the information about the mixture should be continuous and be given in real time. These conditions imply that no method that requires the removal of a test sample from the bulk of the coolant would be suitable. It is apparant that the measurement system would therefore be physically included in the cooling network of the reactor.

In this thesis a novel device as reported in (8) is applied to the problem of determining the dielectric constant. The device consists of an open, cylindrical cavity which is resonant in the microwave frequency region. The cavity is connected to and is concentric with the pipe that transports the coolant as shown in Fig. 1. From an external observation the cavity will appear as simply a stepped increase in the diameter of the pipe.

Closed form solutions for the rf fields in stepped cylindrical waveguides have been attempted previously for various applications in communication systems (2-4). No attempt has been made, however, to analyse these structures when a pair of such steps are so arranged as to form a single-mode, open resonator using the section of larger size waveguide. Nor has there been any attempt to

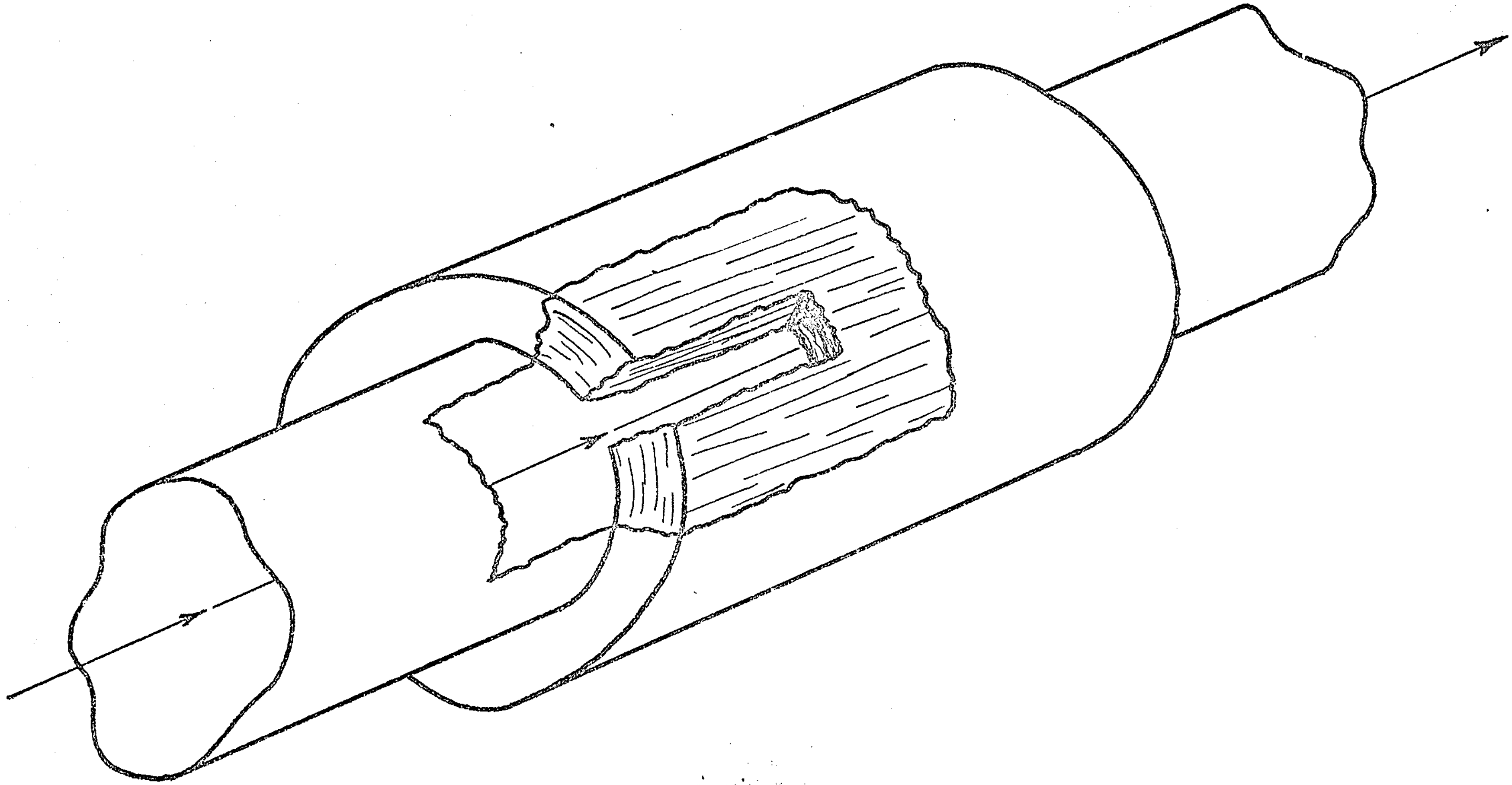

Fig. 1

General view of the void fraction monitor with a section of the conducting wall removed to show the dielectric annulus in the stepped region. The arrows indicate the flow of oil through the monitor.

analyse such resonators as microwave sensors for the purpose of relating the electrical parameters in real time to the physical properties of a material flowing continuously through the smaller size waveguide.

Open cavity resonators have been used for continuous measurement of material characteristics previously. Thorn and Straiton (5) and Wenger and Smetana (6) have designed and tested such devices for the measurement of various properties of smoke and hydrogen gas. These two resonant structures are similar in their designs in that lengths of cylindrical pipes are used to form the resonant section and the end sections which transport the material and which operate below the cut-off frequency of the dominant mode of the resonant section. These designs, however, create an undesirable disturbance in the flow pattern of the fluid to be investigated. More recently, Castle and Roberts (7) employed a design that would give continuous measurement data on an undisturbed flow of crude oil. However, at reasonable frequencies this method is only applicable to small cross-sectional flow areas of the oil. A structure of similar external geometry to that analysed in this thesis, but not similar internally has also been recently tested and reported by Stuchly et al (8). The internal geometry of this structure is such that the flow is disturbed, however, and the results can only be used as a comparison for a special case of the sensor analysed in this thesis.

In general the resonator should not present any impedance to the flow of the material and particularly any sudden change in pressure due to an abrupt difference in cross-sectional area at the step discontinuities. This is overcome in this thesis by filling the stepped region with a ring-shaped dielectric material such that the cross-section of the smaller pipe is maintained physically, but not electrically through the resonator section. The analysis of the structure is thus more complicated than for a single material resonator. The analysis is therefore generalized to cope with this structure with the understanding that the relative dielectric constant can always be set equal to that of the flowing substance whenever the ring is not needed.

As originally suggested by Hahn (9) and subsequently extended to other problems by Bolle (10) and Bhartia and Hamid (11) the field configuration of the sensor is first determined for the various regions of the sensor. The boundary conditions at the conducting walls and the interface conditions between regions are then applied to give the unique field solution for the total sensor.

1.2 Relation Between Void Fraction and Dielectric Constant

To prove that the proposed method of determining the concentration of materials formed by the decomposition of the coolant is feasible, a mixture of two materials will be investigated. The host material will be the organic coolant which will make up the greater part of the volume. The included material will be gas in the form of small voids (bubbles) which will make up the lesser part of the volume. To relate the concentration of the voids to the total volume of the mixture, a ratio called the void fraction is defined as follows:

$$\text{void fraction } (v) = \frac{\text{volume of voids in the mixture}}{\text{total volume of the mixture}} \qquad (1.2.1)$$

where the total volume of the mixture is the volume of the host material plus the volume of the voids. The void fraction can vary between 0.0 (no voids present) to 1.0 (no host material present) although for practical considerations the void fraction will be in the region from 0.0 to 0.1. The sensor of Fig. 1 is designed to allow for an accuracy of better than $\pm$ 0.001 in the determination of the void fraction in the region of practical interest.

The inclusion of a small volume of a dielectric material in the larger volume of a second dielectric alters the field structure present in the second material. This effect has been studied by perturbation theory (12) and the results are well known. When many small inclusions or voids are present the effect of each separate inclusion on the field structure would be difficult if not impossible to analyse and certainly time-consuming to compute. As an example for a total volume of 1 cubic meter, a void fraction of only 0.01, and uniform voids with the fairly large radius of 1 mm would require the analysis of approximately two and a half million perturbations.

To allow for a more practical, but possibly less rigorous solution of the problem , the mixture can be replaced by a homogeneous material of equivalent dielectric properties. Therefore, as the void fraction of the mixture changes so would the dielectric properties of the equivalent material.

The above technique has been substatiated both theoretically and practically by many authors (13-15). These authors have derived relationships between the void fraction and the equivalent dielectric constant but all are based on the following five assumptions:

1. all inclusions should be equally sized and should be small compared to a wavelength of the field,

2. the total void fraction should be small (usually less than 0.1),

3. the voids should be evenly distributed through the total volume,

4. the shapes of all the voids should be roughly the same, and

5. if the general shape of the voids is unsymmetrical, then the orientations will be known.

In addition to the above assumptions, some of the relations take into account the polarization effects between voids and between void and host material.

In the case of a gas-organic coolant mixture at the temperature and pressure mentioned previously, there is definite certainty that the voids will be consistantly small, evenly distributed, and generally spherical. Since the sensor is designed only to operate in the range of void fractions from 0.0 to 0.05 the second assumption is also satisfied.

It was decided that Böttcher's formula for the effective dielectric constant for a two material mixture would provide sufficient accuracy for the needs of this study. Stuchly et al. also used Böttcher's relation, so use of it in this study would be consistent if a comparison is to be done for the special case described later. This formula takes into account of a small polarization effect and appears to be more accurate for this mixture than some of the others.

The form of Böttcher's relation used in this investigation is:

$$\varepsilon_m = \varepsilon_c - 3v\varepsilon_m \left(\frac{\varepsilon_c - \varepsilon_\alpha}{2\varepsilon_m + \varepsilon_\alpha} \right) \qquad (1.2.2)$$

where

ε_c is the relative dielectric constant of the coolant

ε_α is the relative dielectric constant of the gas voids

ε_m is the relative dielectric constant of the equivalent material.

For small values of void fraction ($v < 0.05$), Böttcher's relation can almost exactly be approximated by a straight line. This fact is important as it leads to linearity of the resonant frequency-void fraction curves presented later in this thesis. Fig. 2 shows the curves for the equivalent relative dielectric constant for various values of ε_c with ε_α equal to one.

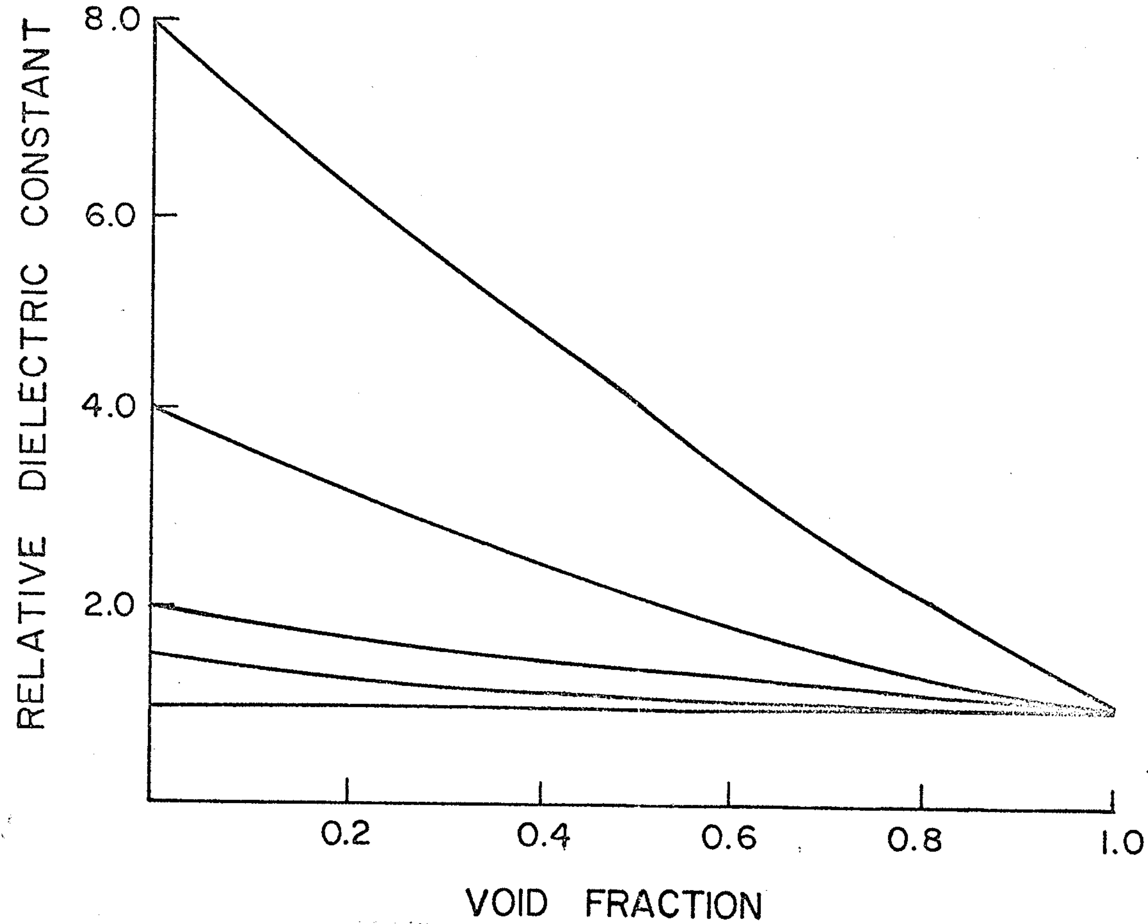

Fig. 2

Curves of Bottcher's equation for values of void fraction from 0.0 to 1.0. The relative permittivity of the flowing materials are 1.0, 1.5, 2.0, 4.0 and 8.0 while that of the voids of 1.0.

2. THEORETICAL ANALYSIS

2.1 Principles of Operation

Although, as mentioned previously, the principle of microwave open-ended cavities has been employed for some time to monitor the indices of refraction of gases and the permittivity of liquids and gases, the present sensor was mainly developed for monitoring the void fraction of organic coolants used in some modern nuclear reactors. Since these coolants are transported at very high temperatures and pressures, the void fraction has to be monitored with little uncertainty in the range of 0.0 to 0.05 for safety and other operational reasons.

For the selected frequency of operation, the circular waveguides at both ends of the sensor section, formed by the coolant piping, operate below cut-off while the sensor section is designed to operate as a resonant cavity.

For small values of the void fraction, the resulting change in the relative dielectric constant of the mixture caused by a variation in void fraction is expected to remain small and along a linear relationship (i.e., in the perturbation region). Since a change in the dielectric constant of the mixture results in a change in the resonant frequency and Q-factor of the open-cavity it is possible in principle to retrieve the void fraction in real time by terminal measurements using standard techniques.

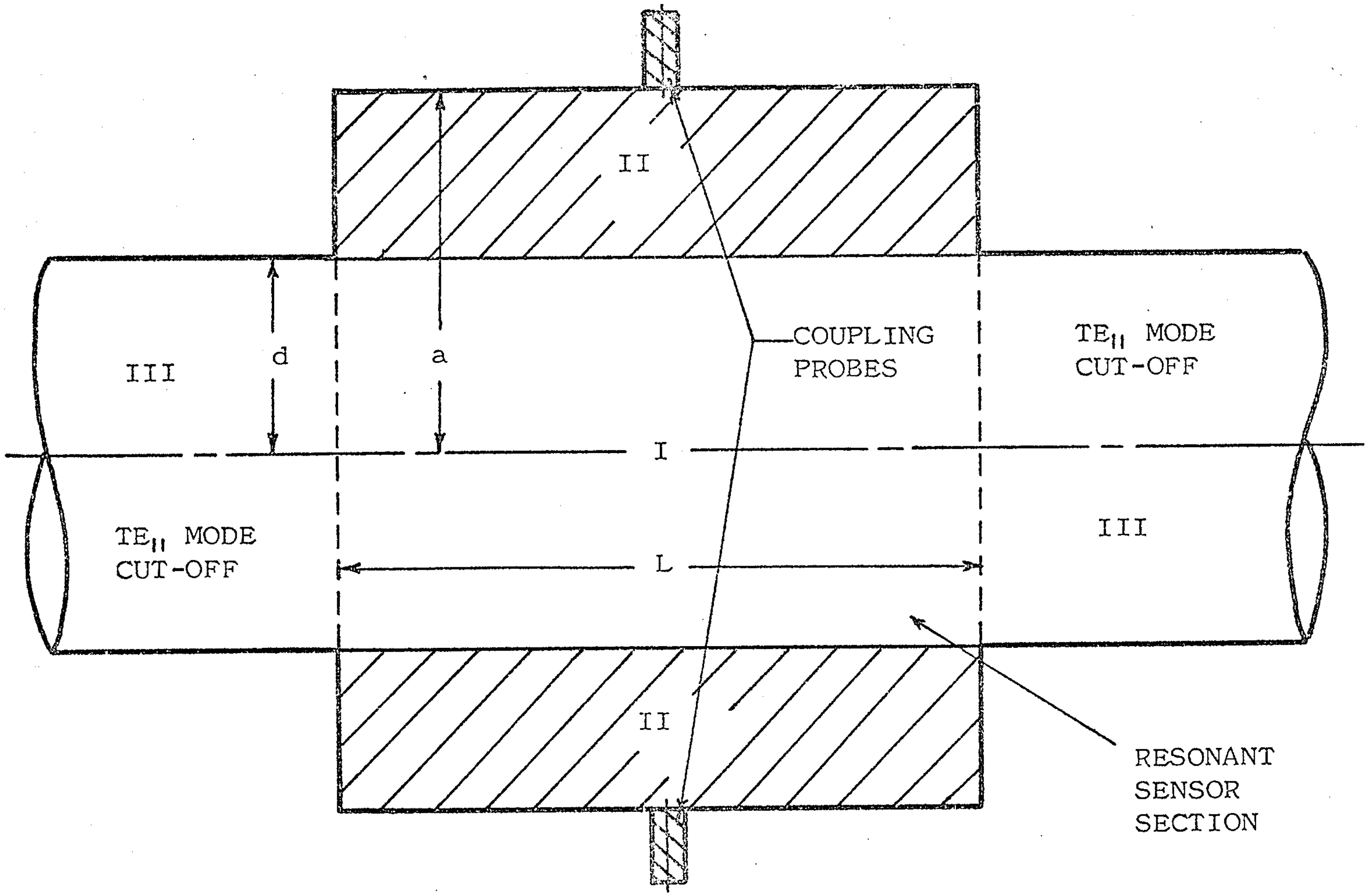

Fig. 3

Longitudinal cross-section of the monitor showing the three regions and the appropriate dimension.

2.2 Formulation of the Problem

Consider the open cavity resonator shown in Fig. 3 where a circular cylindrical waveguide of radius d is enlarged to radius a over the axial section from $z = 0$ to $z = L$. The walls are assumed perfectly conducting and the interior space is filled with a dielectric with voids in regions I and III and a solid dielectric ring in region II. The three regions, as referred to above, are defined as:

$$\begin{array}{llll} \text{region I} & 0 \le r \le d; & 0 \le \phi \le 2\pi; & 0 \le z \le L \\ \text{region II} & d \le r \le a; & 0 \le \phi \le 2\pi; & 0 \le z \le L \\ \text{region III} & 0 \le r \le d; & 0 \le \phi \le 2\pi; & z \le 0 \text{ and } z \ge L \end{array} \qquad (2.2.1)$$

The structure has complete symmetry about the z axis in the cylindrical co-ordinate system (r, ϕ, z) and the time dependance $(e^{j\omega t})$ is assumed and suppressed throughout.

The concentric dielectric layers in the sensor section produce neither pure TE nor pure TM modes, but rather a composite of the two (16, 17). The solutions for the axial and radial components of the magnetic field may be expanded in terms of the partial TM and TE modes as follows:

$$H_z = \frac{1}{\hat{z}} \left(\frac{\partial^2}{\partial z^2} + k^2\right) \psi^E \qquad (2.2.2)$$

$$H_r = \frac{1}{r} \frac{\partial \psi^M}{\partial \phi} + \frac{1}{\hat{z}} \frac{\partial^2 \psi^E}{\partial r \partial z} \qquad (2.2.3)$$

where $\hat{z}$ is the characteristic impedance of the material

ψ^E is the electric wave function

ψ^M is the magnetic wave function

Region I:

$$\psi_I^M = \sum_{q=1}^{\infty} A_{mq} J_m(k_q r) \cos m\phi \; \{ \cos\alpha_q z + A'_{mq} \sin\alpha_q z \} \;, \; m=0,1,2,\ldots \tag{2.2.4}$$

$$\psi_I^E = \sum_{q=1}^{\infty} B_{mq} J_m(k_q r) \sin m\phi \; \{ \cos\alpha_q z + B'_{mq} \sin\alpha_q z \}, \; m=0,1,2,.. \tag{2.2.5}$$

for modes that are symmetrical around $z = \frac{L}{2}$ we have

$$A'_{mq} = B'_{mq} = \frac{1 - \cos \alpha_q L}{\sin \alpha_q L} \tag{2.2.6}$$

for modes that are asymmetrical around $z = \frac{L}{2}$ we have

$$A'_{mq} = B'_{mq} = \frac{-1 - \cos \alpha_q L}{\sin \alpha_q L} \tag{2.2.7}$$

where $k^2 = k_o^2 \, \varepsilon_I$ (2.2.8)

$= k_q^2 + \alpha_q^2$ (2.2.9)

$k_o = 2\pi/\lambda_o$ (2.2.10)

$\hat{z}_I = j\omega \mu_I$

Hence

$$H_{zI} = -\sum_{q=1}^{\infty} \frac{B_{mq}}{\hat{z}_I} k_q^2 \, J_m(k_q r) \sin(m\phi) \; \{ \cos\alpha_q z + B'_{mq} \sin\alpha_q z \} \tag{2.2.11}$$

$$H_{rI} = -\sum_{q=1}^{\infty} \Big[A_{mq} \frac{m}{r} J_m(k_q r) \; \{ \cos\alpha_q z + A'_{mq} \sin\alpha_q z \}$$

$$+ B_{mq} k_q \alpha_q J'_m(k_q r) \{ \sin\alpha_q z - B'_{mq} \cos\alpha_q z \} \Big] \sin m\phi \;, m=0,1,2,\ldots \tag{2.2.12}$$

where J_m is the Bessel function and the prime superscript above the Bessel function denotes differentiation with respect to the total argument.

Region II:

$$\psi_{II}^M = \sum_{s=1}^{\infty} C_{ms} \; \{ J_m(k_s r) + R_{ms}^M N_m(k_s r) \} \cos m\phi \; \{ \cos\beta_s z + C'_{ms} \sin\beta_s z \},$$

$$m = 0, 1,2,\ldots\ldots \tag{2.2.13}$$

$$\psi^E_{II} = \sum_{s=1}^{\infty} D_{ms} \{J_m(k_s r) + R^E_{ms} N_m(k_s r)\} \sin m\phi \{\sin \beta_s z + D'_{ms} \cos \beta_s z\}, \; m = 0, 1, 2, \ldots \quad (2.2.14)$$

where
$$k^2_{II} = k^2_o \varepsilon_{II}$$
$$= k^2_s + \beta^2_s \quad (2.2.15)$$
$$\hat{z}_{II} = j\omega\mu_{II} \quad (2.2.16)$$

and N_m are the Neumann functions. Hence

$$H_{zII} = -\sum_{s=1}^{\infty} \frac{D_{ms}}{\hat{z}_{II}} k^2_s \{J_m(k_s r) + R^E_{ms} N_m(k_s r)\} \sin m\phi \{\sin\beta_s z + D'_{ms} \cos\beta_s z\} \quad (2.2.17)$$

$$H_{rII} = -\sum_{s=1}^{\infty} \Big[C_{ms} \frac{m}{r} \{J_m(k_s r) + R^E_{ms} N_m(k_s r)\} \{\cos\beta_s z + C'_{ms} \sin\beta_s z\} + \frac{D_{ms}}{\hat{z}_{II}} k_s \beta_s \{J'_m(k_s r) + R^E_{ms} N'_m(k_s r)\} \{D'_{ms} \sin\beta_s z - \cos\beta_s z\}\Big] \sin m\phi \quad (2.2.18)$$

Region III:

In this section the field is composed of only TE modes.

$$\psi^E_{III} = \sum_{n=1}^{\infty} G_{mn} J_m(k_n r) \left\{\begin{matrix}\sin m\phi \\ \cos m\phi\end{matrix}\right\} \{\cos \gamma_n z + G'_{mn} \sin \gamma_n z\}, \quad m = o, 1, 2, \ldots \quad (2.2.19)$$

for modes symmetric around $z = \frac{L}{2}$ we have

$$G'_{mn} = \frac{1 - \cos \gamma_n L}{\sin \gamma_n L} \quad (2.2.20)$$

for modes asymmetric around $z = \frac{L}{2}$ we have

$$G'_{mn} = \frac{-1 - \cos \gamma_n L}{\sin \gamma_n L} \quad (2.2.21)$$

where $$k_{III}^2 = k_o^2 \varepsilon_{III}$$

$$= k_n^2 + \gamma_n{}^2 \tag{2.2.22}$$

$$\hat{z}_{III} = j\omega\mu_{III} \tag{2.2.23}$$

since $\varepsilon_{III} = \varepsilon_I$ and $\mu_{III} = \mu_I$ we obtain

$$k_{III}^2 = k_I^2 \text{ and } \hat{z}_{III} = \hat{z}_1 \tag{2.2.24}$$

and hence

$$H_{zIII} = \sum_{n=1}^{\infty} \frac{G_{mn}}{\hat{z}_{III}} k_n^2 J_m(k_n r) \begin{pmatrix} \sin m\phi \\ \cos m\phi \end{pmatrix} \{ \cos\gamma_n z + G'_{mn} \sin\gamma_n z \} \tag{2.2.25}$$

$$H_{rIII} = -\sum_{n=1}^{\infty} \frac{G_{mn}}{\hat{z}_{III}} k_n \gamma_n J'_m(k_n r) \begin{pmatrix} \sin m\phi \\ \cos m\phi \end{pmatrix} \{ \sin\gamma_n z - G'_{mn} \cos\gamma_n z \} \tag{2.2.26}$$

2.3 Application of Boundary Conditions

The field solutions for regions I, II, and III are general. To specify the unique solution for these regions, the appropriate boundary conditions must be applied. The conditions at the conducting walls to be imposed on the magnetic and electric fields in the three regions are given by

$$H_{r_{II}} = 0 \qquad \text{at } r = a \tag{2.3.1}$$

$$\left.\begin{aligned} E_{r_{II}} &= 0 \\ H_{z_{II}} &= 0 \end{aligned}\right\} \quad \text{at } z = 0 \text{ and } z = L \tag{2.3.2}$$

$$H_{r_{III}} = E_{z_{III}} = 0 \quad \text{at } r = d \tag{2.3.3}$$

These conditions, upon application to the appropriate field expressions, lead to the following relations

$$R^M_{ms} = -\frac{J_m(k_s a)}{N_m(k_s a)} \tag{2.3.4}$$

$$R^E_{ms} = -\frac{J'_m(k_s a)}{N'_m(k_s a)} \tag{2.3.5}$$

$$C'_{ms} = 0 \tag{2.3.6}$$

$$D'_{ms} = 0 \tag{2.3.7}$$

$$\beta_s = \frac{s\pi}{L} \tag{2.3.8}$$

$$J'_m(k_n d) = 0 \tag{2.3.9}$$

These relations are to be substituted into the expressions (2.2.11), (2.2.12), (2.2.17), and (2.2.18). Because of the length of these expressions, they will not be rewritten here.

2.4 Application of Interface Conditions

The interface conditions, special cases of boundary conditions, are applied whenever two regions meet at a common boundary. They are applied to insure that the fields do not have discontinuities where none are allowed.

The following are the two conditions:

1) all tangential field components (Ez, $E\phi$, Hz, $H\phi$) are equal on either side of the interface between regions I and II (i.e., at $r = d$; $0\leq\phi\leq 2\pi$; $0\leq z\leq L$), an interface between two different dielectrics; and

2) all field components are equal on either side of the interface between regions I and III (i.e., at $z = 0$ and $z = L$; $r \leq d$; $0 \leq \phi \leq 2$), actually an imaginary interface where the dielectrics on either side of the boundary are the same.

Between regions I and II the orthogonality property of trigonometric functions is applied to the following expression resulting from the first interface condition:

$$\int_0^L H_{z_I}\Big|_{r=d} \sin \frac{\ell\pi}{L} z \, dz = \int_0^L H_{z_{II}}\Big|_{r=d} \sin \frac{\ell\pi}{L} z \, dz \qquad \ell = 1,2,3,\ldots \tag{2.4.1}$$

On substituting the appropriate field expressions, (2.4.1) becomes

$$\sum_{q=1}^{\infty} \frac{B_{mq}}{\hat{z}_{II}} k_q J_m(k_q d) \sin m\phi \int_0^L \{\cos\alpha_q z \quad B'_{mq} \sin\alpha_q z\} \sin \frac{\ell\pi}{L} z \, dz$$

$$= \sum_{s=1}^{\infty} \frac{D_{ms}}{\hat{z}_{II}} k_s \{J_m(k_s d) \; R^E_{ms} N_m(k_s d)\} \sin m\phi \int_0^L \sin \frac{s\pi}{L} z \sin \frac{\ell\pi}{L} z \, dz \tag{2.4.2}$$

Because of the orthogonality property of the trigonometric functions the integral on the right side of (2.4.1) is non-zero only for values of $s = \ell$ and thus the values of the constants $D_{m\ell}$ are given by

$$D_{m\ell} = \frac{\hat{z}_{II}}{\hat{z}_I} \sum_{q=1}^{\infty} B_{mq} \left(\frac{k_q}{k_\ell}\right)^2 \frac{J_m(k_q d)}{\{J_m(k_\ell d) + R^E_{m\ell} N_m(k_\ell d)\}} \frac{L}{2}$$

$$\times \frac{\alpha_q^{\,2}}{\alpha_q^2 - \left(\frac{\ell\pi}{L}\right)^2} \left\{ (-1)^{\ell} \sin \alpha_q L + B'_{mq} \left[1 - (-1)^{\ell} \cos \alpha_q L \right] \right\} \qquad (2.4.3)$$

Similarly, application of the orthogonality property on the longitudinal component of the electric field in the analogous expression

$$\int_0^L E_{z_I}\Big|_{r=d} \cos \frac{\ell\pi}{L} z \, dz = \int_0^L E_{z_{II}}\Big|_{r=d} \cos \frac{\ell\pi}{L} z \, dz \qquad (2.4.4)$$

gives the values of the constants $C_{m\ell}$

$$C_{m\ell} = \frac{\hat{y}_{II}}{\hat{y}_I} \sum_{q=1}^{\infty} A_{mq} \left(\frac{k_q}{k_\ell}\right)^2 \frac{J_m(k_q d)}{J_m(k_\ell d) + R^M_{m\ell} N_m(k_\ell d)} \frac{L}{2}$$

$$\times \left\{ (-1)^{\ell} \sin \alpha_q L + A'_{mq} \left[1 - (-1)^{\ell} \cos \alpha_q L \right] \right\} \frac{a_q^2}{\alpha_q^2 - \left(\frac{\ell\pi}{L}\right)^2} \qquad (2.4.5)$$

where $\hat{y}_I = j\omega\varepsilon_I$ and $\hat{y}_{II} = j\omega\varepsilon_{II}$ the characteristic admittances of the dielectrics

Between regions I and III the orthogonality property of Bessel functions is applied to the following expression resulting from the second interface condition:

$$\int_0^d H_{z_I}\Big|_{r=d} J_m\left(\frac{k'_{mi}}{d} r\right) r dr = \int_0^d H_{z_{II}}\Big|_{r=d} J_m\left(\frac{k'_{mi}}{d} r\right) r dr, \qquad i = 1,2,3,\ldots \qquad (2.4.6).$$

where k'_{mi} satisfied the relation $J'_m(k'_{mi}) = 0$ due to equation (2.3.9). By substituting the appropriate expressions for the longitudinal component of the magnetic field, we obtain

$$\sum_{q=1}^{\infty} \frac{B_{mq}}{\hat{z}_I} k_q^2 \sin m\phi \int_0^d J_m(k_q r)\, J_m\left(\frac{k'_{mi}}{d} r\right) r dr$$

$$= \sum_{q=1}^{\infty} \frac{G_{mt}}{\hat{z}_{III}} \left(\frac{k'_{mt}}{d}\right)^2 \sin m\phi \int_0^d J_m\left(\frac{k'_{mt}}{d} r\right) J_m\left(\frac{k'_{mi}}{d} r\right) r dr \qquad (2.4.7)$$

for the values of $t = i$, the integral on the right is non-zero. When the integrals are evaluated the constants G_{mi} can be determined from the expression

$$G_{mi} = \frac{2}{k'^2_{mi} - m^2} \sum_{q=1}^{\infty} B_{mq} k_q^2 \frac{d}{k_q^2 - \left(\frac{k'_{mi}}{d}\right)^2} \frac{J'_m(k_q d)}{J_m(k'_{mi})} \qquad (2.4.8)$$

2.5 Eigenvalues of the Sensor

The constants $C_{m\ell}$, $D_{m\ell}$, and G_{mi} calculated in the previous section are used to determine the fields in the sensor. To determine the eigenvalues (k_q) of the cavity, the interface conditions between regions I and II are arranged in matrix form. As there are two wave functions determining the field components (due to the non-existence of pure modes), the matrix is found to be a 4 X 4 square. When the determinant of this matrix is zero, the sensor is at resonance and the eigenvalues and resonant frequencies can be found.

The form of the determinant is given below where the superscript M denotes field components derived from the magnetic wave functions and the superscript E denotes those derived from the electric wave functions:

$$\begin{vmatrix} E^M_{z_I} & 0 & E^M_{z_{II}} & 0 \\ 0 & H^E_{z_I} & 0 & H^E_{z_{II}} \\ E^M_{\phi_I} & E^E_{\phi_I} & E^M_{\phi_{II}} & E^E_{\phi_{II}} \\ H^M_{\phi_I} & H^E_{\phi_I} & H^M_{\phi_{II}} & H^E_{\phi_{II}} \end{vmatrix} = 0 \qquad (2.5.1)$$

Equation (2.5.1) is solved numerically by varying the values of α_q until a solution is found. The values of α_q are related to the eigenvalues k_q by (2.2.9).

3. DERIVED AND CALCULATED RESULTS

3.1 Evaluation of the Q-Factor

Once the fields are known from the previous sections, the Q may be determined from the following basic equation

$$Q = \frac{\omega \times \text{time average of energy stored in cavity}}{\text{energy loss per second}} \qquad (3.1.1)$$

Since at resonance the time average of the energy stored in the electric and magnetic fields are equal, only the energy stored in the electric field (W_e) will be calculated. As the resonator is subdivided into two regions and there are three electric field components associated with the TE and TM modes in each region, the expression for W_e, using standard procedures (18), results in the following six integrals:

$$W_e = \varepsilon\left[I_1 + I_2 + I_3 + I_4 + I_5 + I_6\right] \qquad (3.1.2)$$

where

$$I_1 = \int_0^{2\pi}\int_0^{L}\int_0^{d} E_{r_I} \cdot E_{r_I}^* \; r dr\, dz\, d\phi \qquad (3.1.3)$$

$$I_2 = \int_0^{2\pi}\int_0^{L}\int_0^{d} E_{z_I} \cdot E_{z_I}^* \; r dr\, dz\, d\phi \qquad (3.1.4)$$

$$I_3 = \int_0^{2\pi}\int_0^{L}\int_0^{d} E_{\phi_I} \cdot E_{\phi_I}^* \; r dr\, dz\, d\phi \qquad (3.1.5)$$

$$I_4 = \int_0^{2\pi}\int_0^{L}\int_d^{a} E_{r_{II}} \cdot E_{r_{II}}^* \; r dr\, dz\, d\phi \qquad (3.1.6)$$

$$I_5 = \int_0^{2\pi}\int_0^{L}\int_d^{a} E_{z_{II}} \cdot E_{z_{II}}^* \; r dr\, dz\, d\phi \qquad (3.1.7)$$

$$I_6 = \int_0^{2\pi} \int_0^L \int_d^a E_{\phi_{II}} \cdot E_{\phi_{II}}^* \, r dr \, dz \, d\phi \tag{3.1.8}$$

Using the previous results for the electric field components and performing the integrations we obtain lengthy expressions which are given in the Appendix.

The power dissipated (P_d) in the conducting boundaries of the resonator may be obtained from the magnetic field components tangential to the walls as expressed by the following relation:

$$P_d = \frac{R_m}{2} \left[2I_7 + 2I_8 + 2I_9 + 2I_{10} \right] \tag{3.1.9}$$

where

$$R_m = \left(\frac{\omega\mu_{II}}{2\sigma}\right)^{\frac{1}{2}}$$

σ is the conductance of the material.

$$I_7 = \int_0^{2\pi} \int_d^a H_{\phi_{II}} \Big|_{z=0} r dr \, d\phi \tag{3.1.10}$$

$$I_8 = \int_0^{2\pi} \int_d^a H_{r_{II}} \Big|_{z=0} r dr \, d\phi \tag{3.1.11}$$

$$I_9 = \int_0^{2\pi} \int_0^L H_{z_{II}} \Big|_{r=a} r dz \, d\phi \tag{3.1.12}$$

$$I_{10} = \int_0^{2\pi} \int_0^L H_{\phi_{II}} \Big|_{r=a} r dz \, d\phi \tag{3.1.13}$$

Using the expressions for the magnetic field components in region II as defined previously, and by performing the integrations, lengthy expressions for I_7 to I_{10} are found as given in the Appendix.

The Q was then calculated according to equation (3.1.1) using the values of I_1 to I_{10}. The dimensions used were those given by Stuchly et al. The results are presented in Table 1.

3.2 Numerical Results

In order to evaluate the propagation constants α_q, the determinantal equation (2.5.1) was solved numerically using an IBM System 370 digital computer at the University of Manitoba as an exact solution was not possible in closed form. The numerical method employed used a mesh-halving technique to arrive at a reasonably accurate answer while not consuming too much computing time.

To get a rough map of the values of the determinant, an initial sweep of all integral values of α_q from zero to a determined upper value was done. Using this coarse mesh size, the zeros of the determinantal equation could be determined as shown below and a range of values was determined to which mesh halving was applied.

The zeros were described numerically by the conditions:

i) the arithmetic signs of the values Δ_m and Δ_{m+1} (see Fig. 4a) were opposite

ii) the absolute magnitude of Δ_m was less than the absolute magnitude of Δ_{m-1}

The first condition insures that the two outer points of the mesh border the zero. The second condition convergence to take place about poles of type P2 in Fig. 4a where the mesh points are such that condition (i) is satisfied. Fig. 4a is a graph showing the various types of behavior that the value of the determinant could show. Only

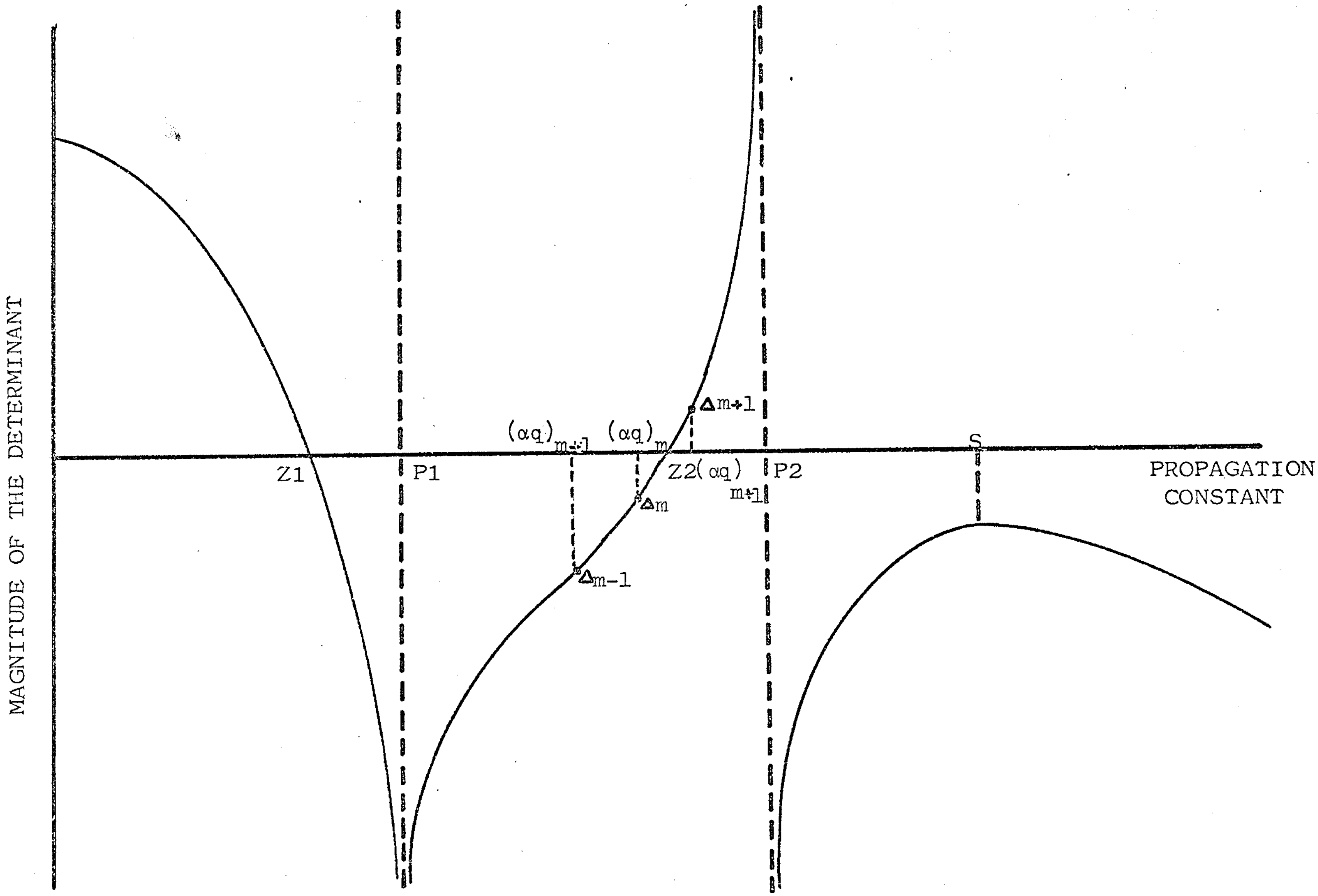

Fig. 4 a

General curve of the value of the determinant as a function of the propagation constant

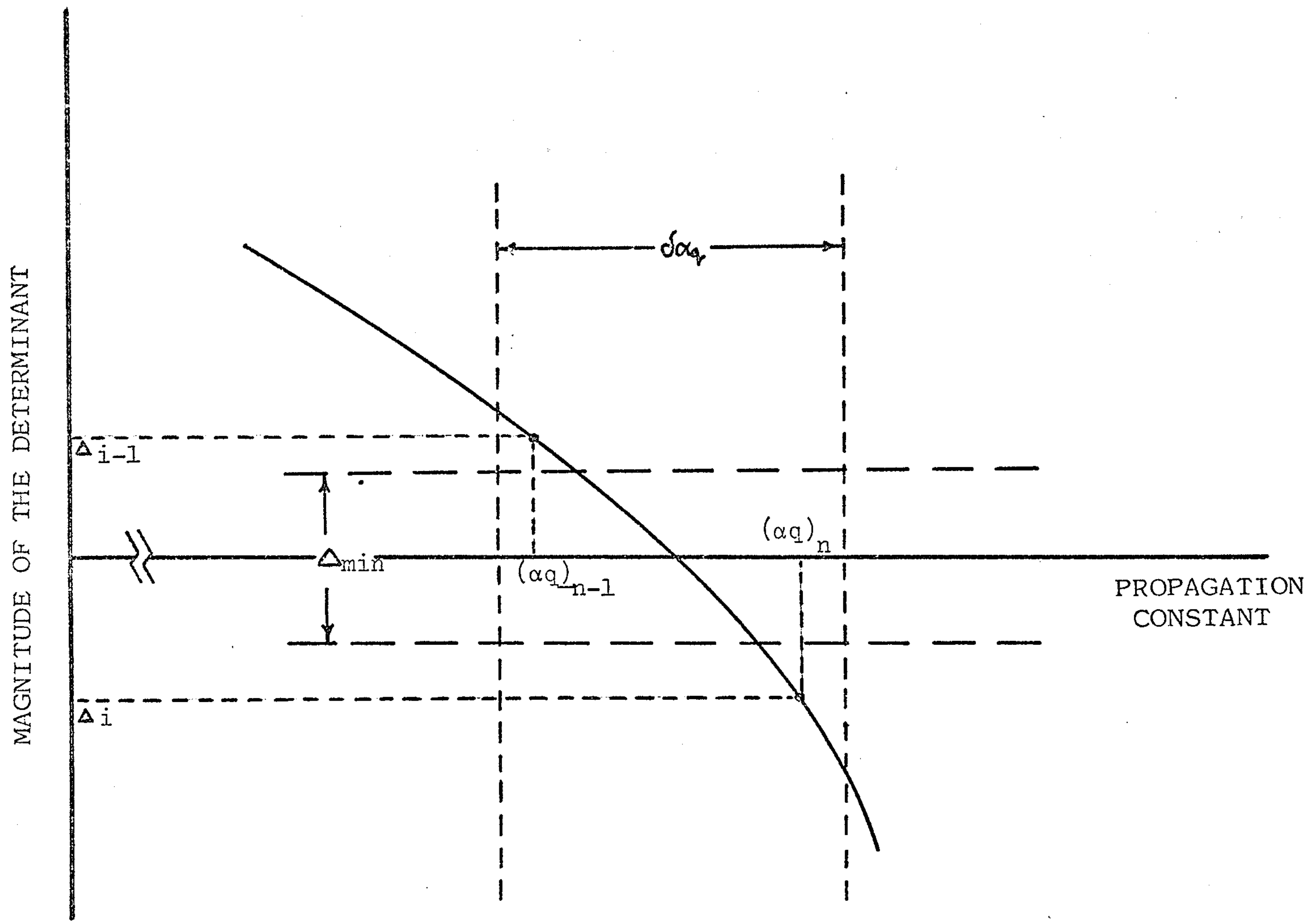

Fig. 4b

Graph of zero with bounding termination conditions zeros of types Z1 or Z2 are true solutions. However, unless the above two conditions were applied convergence also could occur at saddle points (S) and poles of type P1 (one-sided) or P2 (two-sided).

In order to achieve convergence to an acceptable degree of accuracy, while not allowing the computing time to become excessive, two simultaneous conditions were imposed to allow truncation of the convergence process before a numerically exact solution was found. The first condition permitted truncation when the following relational inequality was satisfied:

$$(\alpha q)_n - (\alpha q)_{n-1} < \delta\alpha_q \qquad (3.2.1)$$

where $(\alpha q)_n$ is the nth value of the propagation value determined, $(\alpha q)_{n-1}$ is the (n-1)th value, and $\delta\alpha q$ is the desired accuracy. It is important to note that Δ_n and Δ_{n-1} will be of opposite sign as they border a zero.

The second condition was imposed according to the inequality.

$$|\Delta i| < \Delta\text{min} \qquad (3.2.2)$$

where Δi is the ith value of the determinant in (2.5.1) and Δmin is the required minimum value. These two conditions form a rectangle about the exact value of the zero as shown in Fig. 4b. The size of the rectangle determines the accuracy of the final answer derived by the numerical technique.

The two conditions allow for a reduction in the computing time while still allowing for an accuracy better than a specified

TABLE I

Material Contained in Region I	II	Q
Coolant with v=0.0 ε_r= 2.5-j0.015	Coolant with v=0.0 ε_r= 2.5-j0.015	168.3
Coolant with v=0.1 ε_r= 2.407-j0.013	Coolant with v=0.1 ε_r= 2.407-j0.013	168.5
Coolant with v=0.1 ε_r= 2.407-j0.013	Dielectric ring ε_r= 2.5-j0.0001	177.1
Empty v= 1.0 ε_r= 1.0	Empty v= 1.0 ε_r= 1.0	3600.0

coolant: ε_r= 2.5-j0.015 for no void condition

walls: aluminum σ= 3.43×10^{7}

permittivities: μ=-$4\pi\times10^{-7}$

Q-factor of the cavity for the sensing mode

Note: due to the small values of ε'' the materials were considered to be lossless in the computations.

limit. As can be seen from Fig. 4b, satisfaction of one condition does not necessarily imply immediate satisfaction of the second. In the numerical solution of this problem, however, the value of Δmin was specified at a sufficiently small size that both conditions (3.2.1) and (3.2.2) could be satisfied almost simultaneously. By choosing appropriate values sufficient accuracy was achieved to allow for determination of the resonant frequency to within the desired limits ($\pm$ 0.1 MHz)

As a first step in solving actual physical problems, the numerical procedure was carried out for the case with L = 0.1270 m, d = 0.0635m and a = 0.07875m with $\varepsilon_I = \varepsilon_{II}$. This special case, with the same material in region II that is in region I, was chosen as the results could be compared with the available experimental data given by Stuchly et al.. The range in void fractions was from 0.00 to 0.05 which corresponds to a range in relative dielectric constants from 2.50 to roughly 2.41 from Böttcher's equation (1.2.2).

To get a good sample of data points the resonant frequency was calculated for eleven points in the void fraction range given above spaced at intervals of 0.005. The calculated values are plotted in Figure 5. As was desired and expected, the graph of the points is roughly a straight line. On comparison with the experimental results available (shown by the crosses in the figure) the agreement is remarkably good. The calculated standard deviation of the difference between the experimental data and the curve derived in this thesis is less than 0.2 MHz. The agreement of these results lends

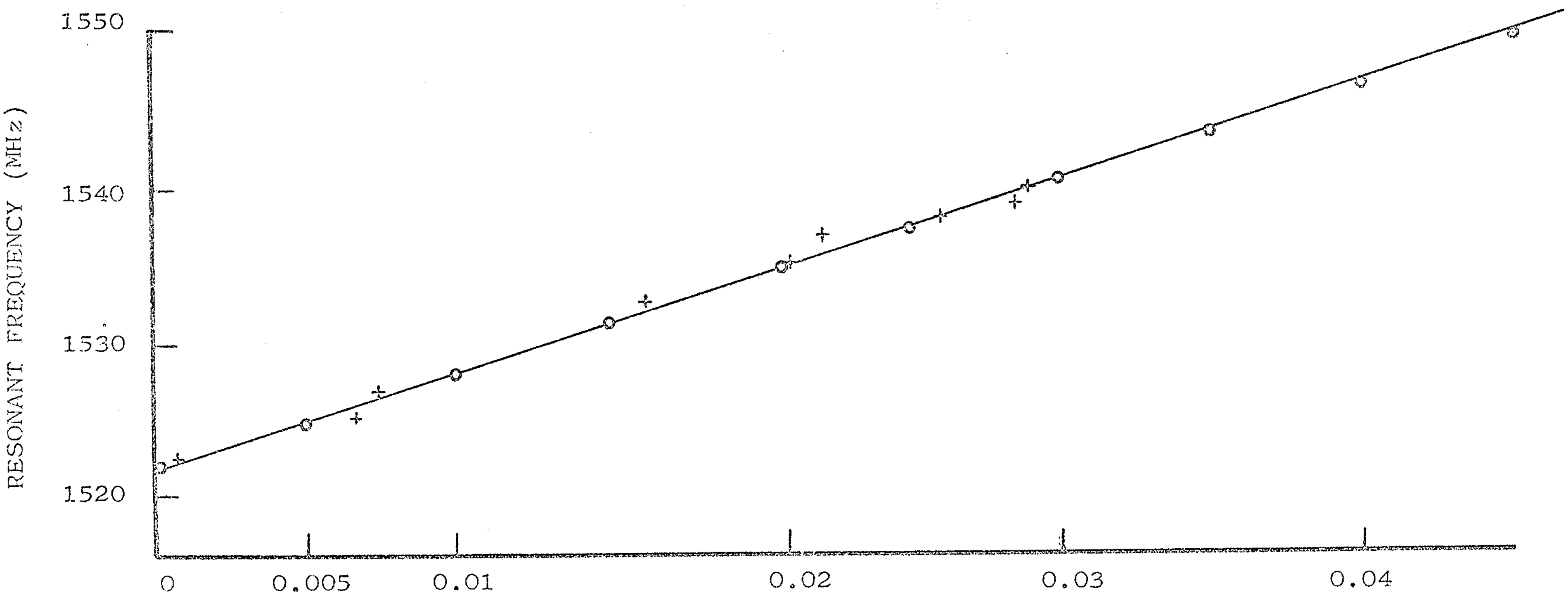

Fig. 5

Resonant frequency of the monitor as a function of void fraction for $\varepsilon_{II} = \varepsilon_{I}$. Circles represent calculated points while the solid line shows the general behaviour of these points. The crosses show the experimental results given by Stuchly et al. (8)

credance to the proposed solution and gives confidence in the results for other cases which are not substantiated by experimental data.

Other values for the relative permittivity of the material within region II were also investigated. Three of the values used were 1.5, 2.5, and 4.24 with the resulting curves presented in Figs. 6-8. As can be seen by a comparison of the solid lines in these figures and the dashed line, there is a reduction in the measurement sensitivity in all cases. However, for the value 2.5 the reduction is minimal. This value is a reasonable compromise between the desired sensitivity and the need for a solid dielectric. In unshown results for values above 4.24, it is evident that the sensitivity decreases. Therefore, as previously mentioned, the optimal value is close to that of the flowing material.

Figures 9 and 10 are representations of the results for sensors with varied size of outer diameter. As can be seen there is some increase in the sensitivity as the diameter is enlarged. Further discussion of this material will be found in the next chapter.

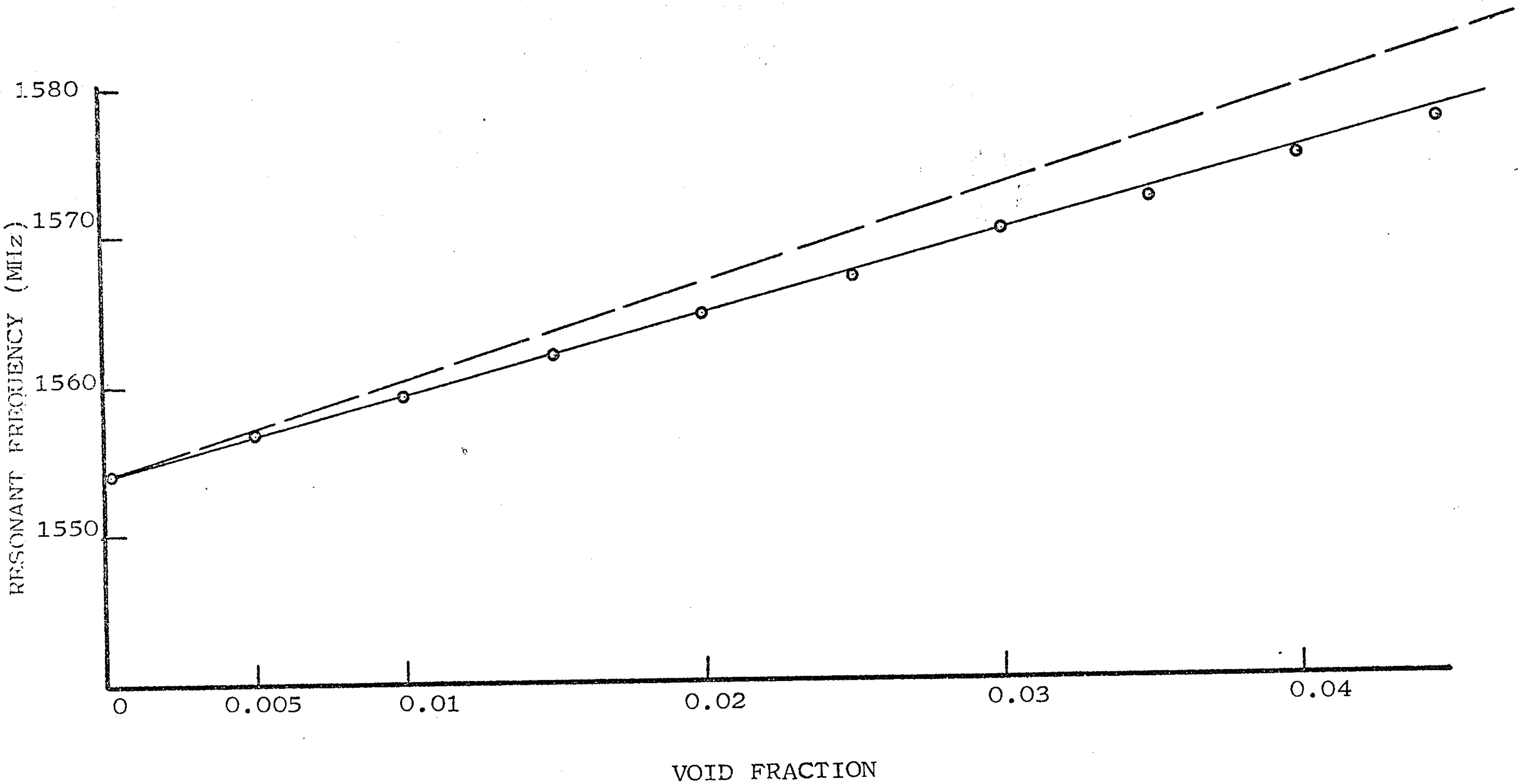

Fig. 6

Resonant frequency of the monitor as a function of the void fraction for $\varepsilon_{II} = 1.5\ \varepsilon_o$. The dashed line is the slope of the line for $\varepsilon_{II} = \varepsilon_I$.

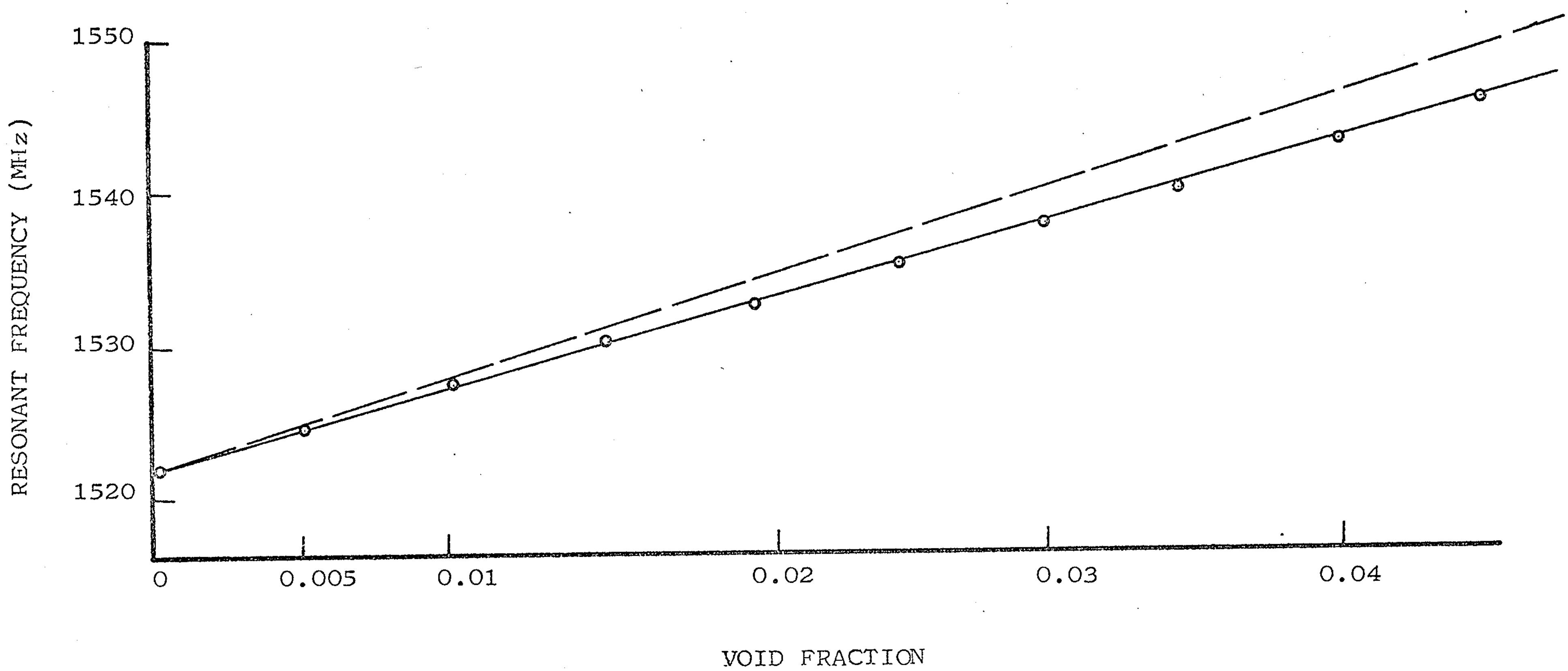

Fig. 7

Resonant frequency of the monitor as
a function of the void fraction for
$\varepsilon_{II} = 2.5\ \varepsilon_o$

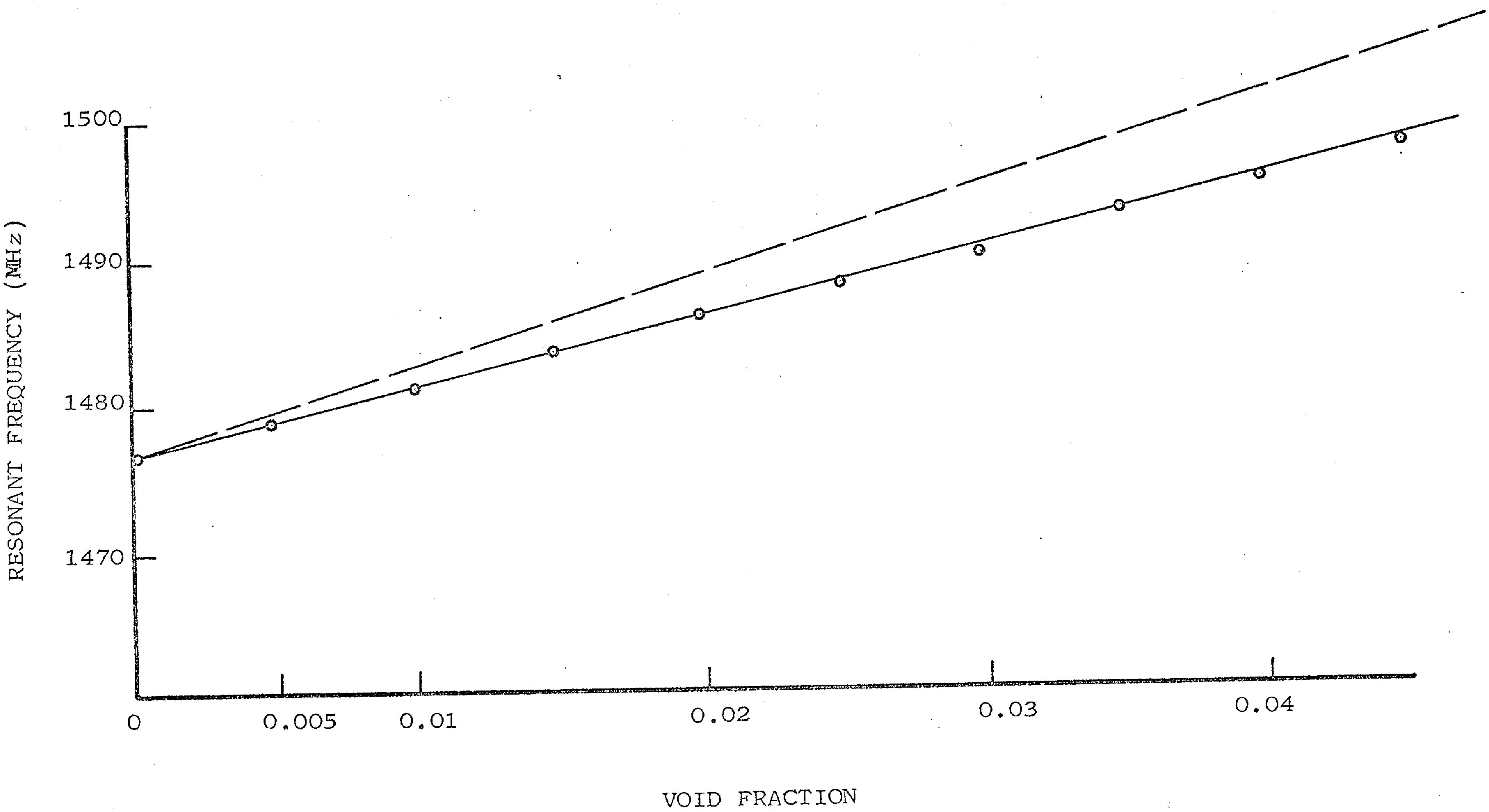

Fig. 8

Resonant frequency of the monitor as a function of the void fraction for $\varepsilon_{II} = 4.24\ \varepsilon_o$.

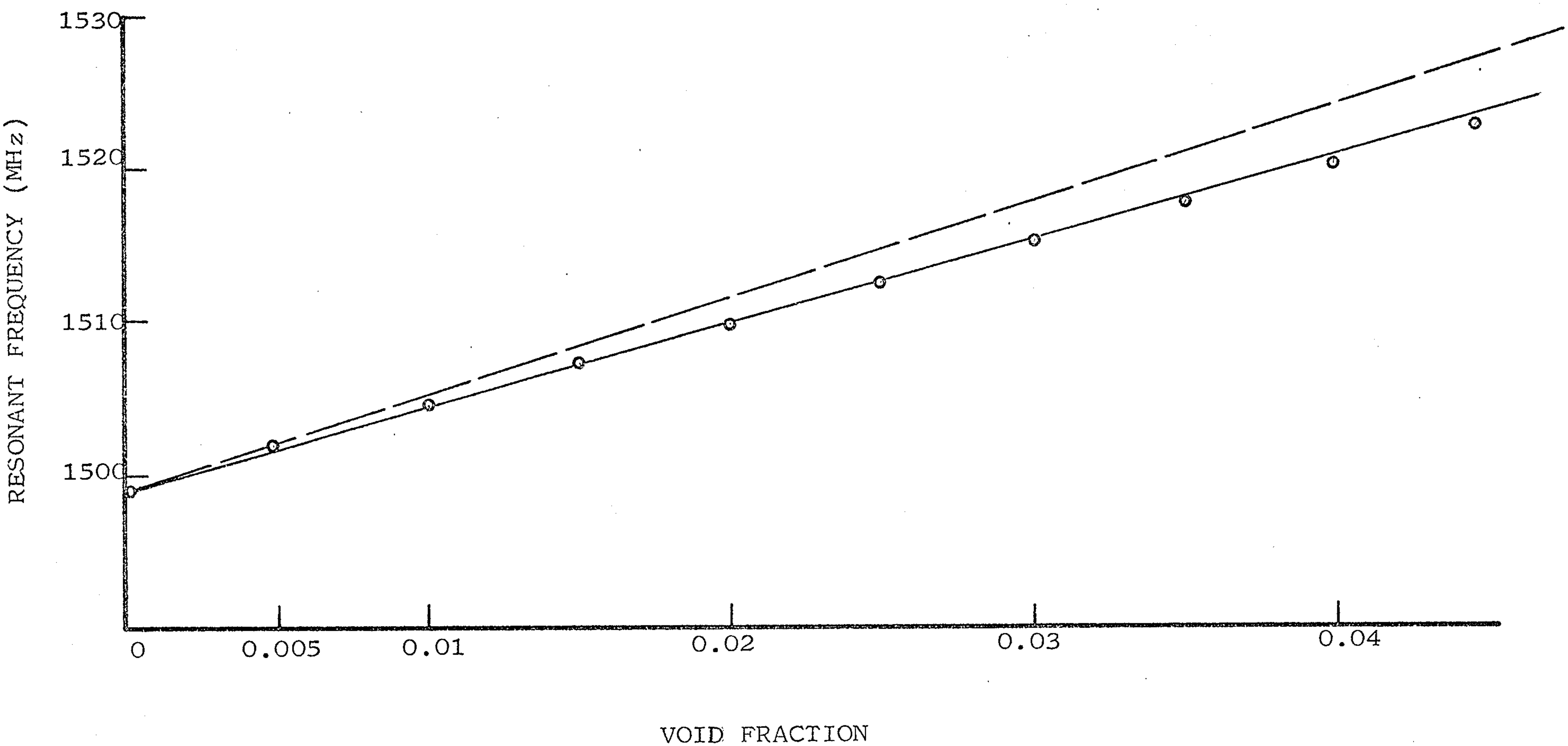

Fig. 9

Resonant frequency of the monitor
as a function of the void fraction
for $\varepsilon_{II} = 2.5\ \varepsilon_o$ and an outer
diameter of 0.0775 m.

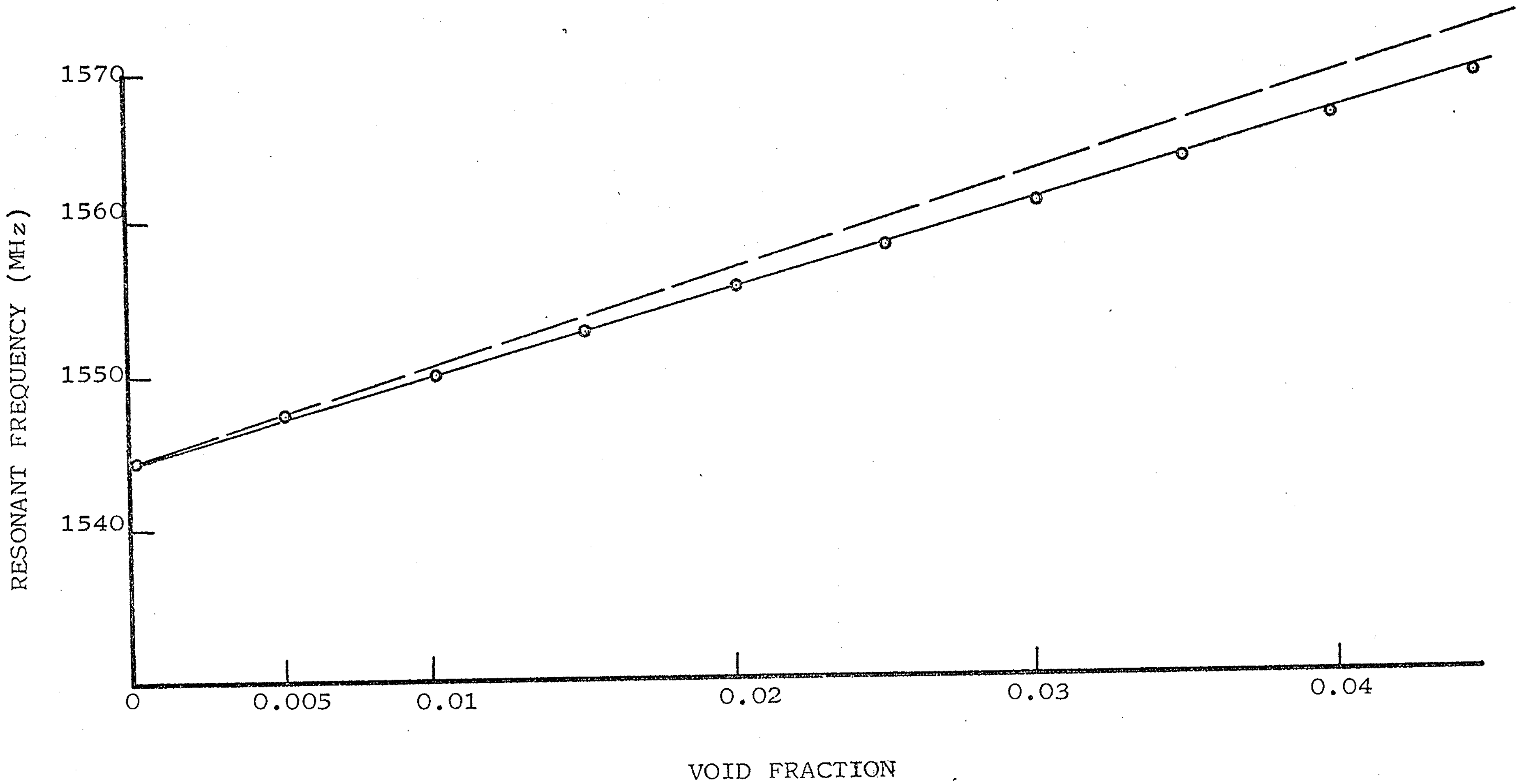

Fig. 10

Resonant frequency of the monitor as a function of the void fraction for $\varepsilon_{II} = 2.5\ \varepsilon_o$ and an outer diameter of 0.080 m.

4. CONCLUSION

4.1 Discussion of Results

Examination of the results presented in the preceding sections shows that the agreement with experimental data for the special case of $\varepsilon_I = \varepsilon_{II}$ is remarkable. The computation time required to achieve this agreement was large though not overly excessive and would lend itself to the design of actual cavities. A large portion of the time was taken in the determination of various Bessel functions which had to be recalculated for every iteration as the argument changed. As the subprograms used were the fastest generating available, little hope of decreasing the computation time by pursuing a course in this direction would be expected.

The number of terms for the expansions in the determinantal equation (2.5.1) used to achieve the specified degree of accuracy was 12 - 15. This was in the vicinity of the range reported by Bhartia and Hamid (11) for a mathematically similar situation based on a simpler geometry where composite (longitudinal) modes were not present as the cavity contained only one dielectric. Reduction in the number of terms would reduce the number of Bessel functions that must be calculated leading to a reduction in the computing time for each iteration. However, a greater number of iterations would have to be done and the end result, in terms of computation time, would only be a slight improvement. It must also be kept in mind that this would also result in a reduction in the resultant accuracy.

The previously-mentioned agreement with experimental data increases the confidence in the results for the more general cases where $\varepsilon_I \neq \varepsilon_{II}$. These results are necessary for expanding the application of the sensor to other flowing materials or mixtures of different materials where knowledge of the volumetric ratios (or void fraction or moisture content in some applications) are desirable and lie within the perturbation range. Foreseen possible uses include measuring the moisture content of butter or sausages and the butterfat content of milk.

As the design specifications of the sensor required only operation within the void fraction range from 0.0 to 0.05, no previous mention was made as to the computed behaviour of the sensor beyond this range. However, for the sake of completeness and possible future use, the range of computation was doubled for some cases. As was mentioned previously, the behaviour of Bottcher's equation for small values of void fraction was nearly linear. This behavior was evident, in the case of the materials discussed in this thesis, up to a value of V equal to 0.05. From Fig. 2 it can be seen that the curves began to curve as the void fraction increased. For an oil with relative permittivity equal to 2.5, the curvature was most noticable in the mid-section of the graph from V equal to 0.2 to V equal to 0.7. As the resonant frequency is dependant on the dielectric constant, as shown in this thesis, the resonant frequency vs. void fraction curves were also expected to show a non-linear behaviour in this region. As no experimental data is available for values of void fraction greater than 0.05, it is impossible to pass comment on the accuracy of the technique for comparatively large values other than to say that the demonstrated agreement for low values could be extrapolated to higher values.

The main problem arising from the extension of this monitoring method into the higher void fraction region is that it is moved out of the perturbation region. The relations between void fraction and dielectric constant are defined and most exact in this region. However, if not as exact determination of material quantities is required, then it is possible to use such a monitor.

Due to the curving of the resonant frequency vs. void fraction curves for larger values of V the sensitivity of the monitor decreases assuming a constant accuracy in the determination of the frequency. This can best be illustrated by a simple example. If the slope of the graph is 0.0025/MHz (i.e., a change of 20 MHz for a void fraction going from 0.0 to 0.05) then with a detection uncertainty of ±0.2 MHz the uncertainty in the determination of V would be ±0.0005. For a slope of only 0.005/MHz then the corresponding uncertainty would be ±0.001. While the first answer is much better than designed for, the second is at the upper limit of the allowed uncertainty. Because of the curving of the graph the latter value of slope may be achieved when the void fraction approaches 0.1. To achieve the best possible accuracy in the determination of the void fraction from actual measured resonant frequency data containing some uncertainty it is thus desirable to have the highest possible change in resonant frequency for a corresponding change in void fraction. This is a consideration that the design engineer must remember.

From the results presented previously, it appears that the highest slope was achieved for the case when there was no dielectric ring present. However, almost as good a result was achieved when a dielectric of relative permittivity equal to 2.5 was inserted. The presence of the dielectric also had the desirable effects described in the introduction. Dielectric constants on either side of this optimum changed not only the slope of the graph but also the originating frequency when the void fraction was zero.

From a design point of view, the results presented suggest that as ε_{II} is made increasingly larger than ε_{I} the electrical volume of the resonator increases while the actual physical volume remains the same; hence explaining the desirable raising of the Q-factor of the cavity. However, this can only be done provided that the resonator is not over-moded since the proposed perturbation is for a single-moded cavity only.

4.2 Further Suggestions

From the results presented in this thesis and, to a certain extent, from the experience drawn from the researching of this technique, some guidelines may be given for the actual designing of the monitors. Also, some suggestions for further research can be realized.

In order to avoid other higher-order modes from interfering with the resulting smaller bandwidth of the desired mode; as the values of ε_{II} is increased; and to keep measurement problems and dielectric losses in mind, the designer must compromise between a higher Q-factor and lower measurement sensitivity. As can be seen in the results given for different permittivity values of the dielectric ring, the optimum value of ε_{II} is one equal to ε_{I}. As the permittivity of the material in the transport region is variable and that of the dielectric ring is constant, an optimum constant value must be chosen. Obviously, each application requires separate computation of these values.

The ratio of the inner to outer diameters was specified to be quite large (above 0.7) for the use intended. However, this value can be varied in other cases. As the ratio decreases the losses through the openings also decrease and the resulting frequency sensitivity should increase. The Q-factor would increase correspondingly. By using a variation of the ratio to achieve an increase in the sensitivity would not cause over-moding as variation of the dielectric constant would. This is due to the smaller influence of the central transport region on the total field of the sensor. The designer therefore has two ways of approaching the optimum design of the monitor.

For the direct application of the monitor to its intended use, or to any similar use, would require more information about the properties of available solid dielectrics. After only a cursory examination, a few materials, such as some types of Corning glass or some resins, were deemed to be suitable. However, due to the severe temperature and pressure conditions present, the long-term behaviour of these materials cannot be forecast. It is hoped that some type of material could be found that would require replacement only after extended periods of time to avoid unnecessary reactor shutdowns.

While the geometry of the monitor suggested in this thesis proved feasible, it is believed that investigation of more complex geometries might lead to a more optimal design. The introduction of a multi-layered shell in place of the single dielectric in region II or the use of a narrow airgap between the dielectric annulus and the cylindrical walls; as investigated by Oliner (19) and Towaij and Hamid (20) for optimum waveguide transmission and antenna design problems; would allow the designer more leeway in the choice of dimensions. The thickness and the choice of suitable dielectrics in the first suggestion are design problems beyond the scope of this thesis. The thickness of an airgap is expected to be critically small and would require precision machining. The use of such geometries would only be a useful modification to the present sensor as long as the resonant frequency vs. void fraction (or other desired quantity) remained linear(within the perturbation range of interest).

Extension of the work of this thesis to multi-material mixtures is also deemed to be a useful area of investigation. A study of this sort would extend the use of such a monitor many-fold. For this type of problem, it is expected that a single measurement of resonant frequency would not determine a unique void fraction. Measurement of the non-dominant mode frequencies would probably supply the necessary additional information. Another possible approach would be the use of a series of open, resonant cavities operating at different frequencies.

The problem, to a reasonable degree of accuracy, has thus been analysed and the designer is armed with the tools in this thesis or in (21) to achieve a suitable device for his unique application.

Appendix

EXPRESSIONS FOR I_1 to I_{10}

The integrals I_1 to I_{10} as defined in section 3.1 are given by the following expressions

$$I_1 = \frac{\pi}{4} \sum_{q=1}^{\infty} [\frac{A_{1q}^2}{\hat{y}_I^2} k_q^2 \alpha_q^2 \{ \frac{L}{2} (1 + A_{1q}'^2) - \frac{1}{4\alpha_q} (1 - A_{1q}'^2) \sin 2\alpha_q L$$

$$- \frac{A_{1q}'}{\alpha_q} \sin^2 \alpha_q L\} \{\frac{d^2}{2} [J_0^2(k_q d) + J_1^2(k_q d) + J_2^2(k_q d) - J_1(k_q d) J_3(k_q d)]$$

$$- 2 \int_0^d J_0(k_q r) J_2(k_q r) r dr] + \frac{A_{1q} B_{1q}}{\hat{y}_I} k_q^2 d^2 \alpha_q \{ \frac{L}{2} (B_{1q}' - A_{1q}')$$

$$- \frac{1}{4\alpha_q} (B_{1q}' + A_{1q}') + \frac{1}{2\alpha_q} (1 - A_{1q}' B_{1q}') \sin^2 \alpha_q L\} \{J_0^2(k_q d) + J_1^2(k_q d)$$

$$- J_2^2(k_q d) + J_1(k_q d) J_3(k_q d)\} + B_{1q}^2 k_q^2 \{ \frac{L}{2} (1 + B_{1q}'^2)$$

$$+ \frac{1}{4\alpha_q} (1 - B_{1q}'^2) \sin 2\alpha_q L + \frac{B_{1q}'}{\alpha_q} \sin^2 \alpha_q L\} \{\frac{d^2}{2} [J_0^2(k_q d) + J_1^2(k_q d)$$

$$+ J_2^2(k_q d) - J_1(k_q d) J_3(k_q d)] + 2 \int_0^d J_0(k_q r) J_2(k_q r) r dr\}]$$

$$+ \frac{\pi}{4} \sum_{q=1}^{\infty} \sum_{\substack{u=1 \\ u \neq q}}^{\infty} [\frac{A_{1q} A_{1u}}{\hat{y}_I^2} k_q k_u \alpha_q \alpha_u \{F_1(q,u) + A_{1q}' A_{1u}' F_2(q,u)$$

$$- A_{1q}' T(u,q) - A_{1u}' T(q,u)\} \{\frac{2d}{k_q^2 - k_u^2} [k_q J_1(k_q d) J_1'(k_u d)$$

$$- k_u J_1'(k_q d) J_1(k_u d)] - \int_0^d [J_0(k_q r) J_2(k_u r) + J_2(k_q r) J_0(k_u r)] r dr$$

$$+ 2\frac{A_{1q}B_{1u}}{\hat{y}_I} k_q k_u \alpha_q \{T(q,u) + B'_{1u}F_1(q,u) - A'_{1q}F_2(q,u)$$

$$- A'_{1q}B'_{1u}\ T(u,q)\} \{\frac{2}{k_q k_u} J_1(k_q d)J_1(k_u d) + \int_0^d [J_0(k_q r)J_2(k_u r)$$

$$- J_2(k_q r)J_0(k_u r)]rdr\} + B_{1q}B_{1u}k_q k_u\{F_2(q,u) + B'_{1q}B'_{1u}\ F_1(q,u)$$

$$+ B'_{1q}\ T(q,u) + B'_{1u}T(u,q)\} \{\frac{2d}{k_q^2-k_u^2} [k_q J_1(k_q d)J'_1(k_u d)$$

$$- k_u J'_1(k_q d)J_1(k_u d)] + \int_0^d [J_0(k_q r)J_2(k_u r) + J_2(k_q r)J_0(k_u r)]rdr\}]$$

$$I_2 = \frac{\pi}{2} \sum_{q=1}^{\infty} \frac{A_{1q}^2}{\hat{y}_I^2}\ k_q^2 d^2 \{ \frac{L}{2}(1 + A'^2_{1q}) + \frac{1}{4\alpha_q} (1 - A'^2_{1q})\ \sin 2\alpha qL$$

$$+ \frac{B'_{1q}}{\alpha_q} \sin^2\alpha_q L\} \{J_1^2(k_q d) - J_0(k_q d)J_2(k_q d)\}$$

$$+ \pi \sum_{q=1}^{\infty} \sum_{\substack{u=1\\u\neq q}}^{\infty} \frac{A_{1q}A_{1u}}{\hat{y}_I^2} \frac{k_q^2 k_u^2}{k_q^2-k_u^2} d\ \{F_2(q,u) + A'_{1q}A'_{1u}F_1(q,u)$$

$$+ A'_{1q}\ T(q,u) + A'_{1u}T(u,q)\} \{k_u J_1(k_q d)J_0(k_u d) - k_q J_0(k_q d)J_1(k_u d)\}$$

$$I_3 = \frac{\pi}{4} \sum_{q=1}^{\infty} [\frac{A_{1q}^2}{\hat{y}_I^2} k_q^2\ \alpha_q^2\ \{\frac{L}{2}(1 + A'^2_{1q})\ \frac{1}{4\alpha_q}(1 - A'^2_{1q})\ \sin 2\alpha\ L$$

$$- \frac{A'_{1q}}{\alpha_q}\ \sin^2\alpha_q L\} \{\frac{d^2}{2} [J_0^2(k_q d) + J_1^2(k_q d) + J_2^2(k_q d)- J_1(k_q d)J_3(k_q d)]$$

$$+ 2 \int_0^d J_0(k_q r)J_2(k_q r)rdr\} - \frac{A_{1q}B_{1q}}{\hat{y}_I} k_q^2 d^2 \alpha_q\{\frac{L}{2} (B'_{1q} - A'_{1q})$$

$$- \frac{1}{4\alpha_q}(B'_{1q} + A'_{1q})\ \sin 2\alpha_q L + \frac{1}{2\alpha_q}(1 - A'_{1q}B'_{1q})\ \sin^2\alpha_q L\} \{J_0^2(k_q d)$$

$$+ J_1^2(k_q d) - J_2^2(k_q d) + J_1(k_q d)J_3(k_q d)\} + B_{1q}^2 k_q^2\ \{\frac{L}{2}\ (1+B'^2_{1q})$$

$$+ \frac{1}{4\alpha_q}(1 - B'^2_{1q}) \sin 2\alpha q L + \frac{B'_{1q}}{\alpha_q} \sin^2\alpha_q L\} \{\frac{d^2}{2}[J_0^2(k_q d) + J_1^2(k_q d)$$

$$+ J_2^2(k_q d) - J_1(k_q d)J_3(k_q d)] - 2\int_0^d J_0(k_q r)J_2(k_q r)rdr\}]$$

$$+ \frac{\pi}{4}\sum_{q=1}^{\infty}\sum_{\substack{u=1\\u\neq q}}^{\infty} [\frac{A_{1q}A_{1u}}{\hat{y}_I^2} k_q k_u \alpha_q \alpha_u \{F_1(q,u) + A'_{1q}A'_{1u}F_2(q,u)$$

$$- A'_{1q}T(u,q) - A'_{1u}T(q,u)\} \{\frac{2d}{k_q^2 - k_u^2} [k_u J_1(k_q d)J'_1(k_u d)$$

$$- k_u J'_1 (k_u d)J_1(k_u d)] + \int_0^d [J_0(k_q r)J_2(k_u r) + J_2(k_u r)J_0(k_q r)]rdr\}$$

$$- 2\frac{A_{1q}B_{1u}}{\hat{y}_I} k_q k_u \alpha_q \{T(q,u) + B'_{1u}F_1(q,u) - A'_{1q}F_2(q,u)$$

$$- A'_{1q}B'_{1u}T(u,q)\} \{\frac{2}{k_q k_u} J_1(k_q d)J_1(k_u d) - \int_0^d [J_0(k_q r)J_2(k_u r)$$

$$- J_2(k_q r)J_0(k_u r)]rdr\} + B_{1q}B_{1u} k_q k_u \{F_2(q,u) + B'_{1q}B'_{1u}F_1(q,u)$$

$$+ B'_{1q}T(q,u) + B'_{1u}T(u,q)\} \{\frac{2d}{k_q^2 - k_u^2} [k_q J_1(k_q d)J'_1(k_u d)$$

$$- k_u J'_1(k_q d)J_1(k_u d)] - \int_0^d [J_0(k_q r)J_2(k_u r) + J_2(k_q r) J_0(k_u r)]rdr\}]$$

$$I_4 = \frac{\pi L}{8}\sum_{s=1}^{\infty} [\frac{C_{1s}^2}{\hat{y}_{II}^2} k_s^2 (\frac{\ell\pi}{L})^2 \{\frac{a^2}{2} [Z_0^2(k_s a) + Z_2^2(k_s a)]$$

$$- \frac{d^2}{2} [Z_0^2(k_s d) + Z_1^2(k_s d) + Z_2^2(k_s d) - Z_1(k_s d)Z_3(k_s d)]$$

$$- 2\int_d^a Z_0(k_s r)Z_2(k_s r)rdr\} + 2\frac{C_{1s}D_{1s}}{\hat{y}_{II}} k_s^2 \frac{\ell\pi}{L} \int_d^a \{Z_0(k_s r) - Z_2(k_s r)\}$$

$$\times \{X_o(k_s r) + X_2(k_s r)\}rdr + D_{1s}^2 k_s^2 \{\frac{a^2}{2} [X_1^2(k_s a) - X_1(k_s a)X_3(k_s a)]$$

$$- \frac{d^2}{2} [X_0^2(k_s d) + X_1^2(k_s d) + X_2^2(k_s d) - X_1(k_s d)X_3(k_s d)]$$

$$+ 2 \int_d^a X_0(k_s r)X_2(k_s r)rdr\}]$$

$$- \frac{\pi L}{8} \sum_{s=1}^{\infty} \sum_{\substack{u=1 \\ u\neq s}}^{\infty} [\frac{C_{1s}C_{1u}}{\hat{y}_{II}^2} k_s k_u (\frac{\ell\pi}{L})^2 \{\frac{2d}{k_s^2-k_u^2} [k_s Z_1(k_s d)Z_1'(k_u d)$$

$$- k_u Z_1'(k_s d)Z_1(k_u d)] + \int_d^a [Z_0(k_s r)Z_2(k_u r) + Z_2(k_s r)Z_0(k_u r)]rdr\}$$

$$+ 2 \frac{C_{1s}D_{1u}}{\hat{y}_{II}} k_s k_u \frac{\ell\pi}{L} \{\frac{a}{k_s^2-k_u^2} [k_u Z_0(k_s a)X_1(k_u a)+ k_u Z_2(k_s a)X_1(k_u a)]$$

$$+ \frac{d}{k_s^2-k_u^2} [k_s Z_1(k_s d) \{X_0(k_u d) + X_2(k_u d)\} - k_u X_1(k_u d)\{Z_0(k_s d)+Z_2(k_s d)\}]$$

$$- \int_d^a [Z_0(k_s r)X_2(k_u r) - Z_2(k_s r)X_0(k_u r)]rdr\} + D_{1s}D_{1u} k_s k_u$$

$$\times \{\frac{2d}{k_s^2-k_u^2} [k_s X_1(k_s d)X_1'(k_u d) - k_u X_1'(k_s d)X_1(k_u d)]$$

$$- \int_d^a [X_0(k_s r)X_2(k_u r) + X_2(k_s r)X_0(k_u r)]rdr\}]$$

$$I_5 = \frac{\pi L}{4} \sum_{s=1}^{\infty} \frac{C_{1s}^2}{\hat{y}_{II}^2} k_s^4\{a^2 Z_0(k_s a)Z_2(k_s a) - d^2 [Z_1^2 (k_s d)$$

$$- Z_0(k_s d)Z_2(k_s d)]\} - \frac{\pi L}{2} \sum_{s=1}^{\infty} \sum_{\substack{u=1 \\ u\neq s}}^{\infty} \frac{C_{1s}C_{1u}}{\hat{y}_{II}^2} \frac{k_s^2 k_u^2}{k_s^2-k_u^2} d\{k_u Z_1(k_s d)Z_0(k_u d)$$

$$- k_s Z_0(k_s d)Z_1(k_u d)\}$$

$$I_6 = \frac{\pi L}{8} \sum_{s=1}^{\infty} [\frac{C_{1s}^2}{\hat{y}_{II}^2} k_s (\frac{\ell\pi}{L})^2 \{\frac{a^2}{2} [Z_0^2(k_s a) + Z_2^2(k_s a)]$$

$$- \frac{d^2}{2} [Z_0^2(k_s d) + Z_1^2(k_s d) + Z_2^2(k_s d) - Z_1(k_s d) Z_3(k_s d)]$$

$$+ 2 \int_d^a Z_0(k_s r) Z_2(k_s r) r dr\} + 2 \frac{C_{1s} D_{1s}}{\hat{y}_{II}} k_s^2 \frac{\ell\pi}{L} \int_d^a \{Z_0(k_s r) + Z_2(k_s r)\}$$

$$x \{X_0(k_s r) - X_2(k_s r)\} r dr + D_{1s}^2 k_s^2 \{\frac{a^2}{2} [X_1^2(k_s a) - X_1(k_s a) X_3(k_s a)]$$

$$- \frac{d^2}{2} [X_0^2(k_s d) + X_1^2(k_s d) + X_2^2(k_s d) - X_1(k_s d) - X_3(k_s d)] - 2 \int_d^a X_0(k_s r) X_2(k_s r) r dr\}$$

$$+ \frac{\pi L}{8} \sum_{s=1}^{\infty} \sum_{\substack{u=1 \\ u \neq s}}^{\infty} [\frac{C_{1s} C_{1u}}{\hat{y}_{II}^2} k_s k_u (\frac{\ell\pi}{L})^2 \{\frac{2d}{k_s^2 - k_u^2} [k_u Z_1(k_u d) Z_1'(k_s d)$$

$$- k_s Z_1'(k_u d) Z_1(k_s d)] + \int_d^a [Z_0(k_s r) Z_2(k_u r) + Z_2(k_s r) Z_0(k_u r)] r dr\}$$

$$- 2 \frac{C_{1s} D_{1u}}{\hat{y}_{II}} k_s k_u \frac{\ell\pi}{L} \{\frac{k_u a}{k_s^2 - k_u^2} [Z_0(k_s a) X_1(k_u a) - Z_2(k_s a) X_0(k_u a)]$$

$$+ \frac{d}{k_s^2 - k_u^2} [k_u X_1(k_u d) \{Z_2(k_s d) - Z_0(k_s d)\} - k_s Z_1(k_s d) \{X_2(k_u d) - X_0(k_u d)\}]$$

$$+ \int_d^a [Z_0(k_s r) X_2(k_u r) - Z_2(k_s r) X_0(k_u r)] r dr\} - D_{1s} D_{1u} k_s k_u$$

$$x \{\frac{2d}{k_s^2 - k_u^2} [k_s X_1(k_s d) X_1'(k_u d) - k_u X_1'(k_s d) X_1(k_u d)]$$

$$- \int_d^a [X_0(k_s r) X_2(k_u r) + X_2(k_s r) X_0(k_u r)] r dr\}]$$

$$I_7 = \frac{\pi}{4} \sum_{s=1}^{\infty} [C_{1s}^2 k_s^2 \{\frac{a^2}{2} [Z_0^2(k_s a) + Z_2^2(k_s a)] - \frac{d^2}{2} [Z_0^2(k_s d)$$

$$+ Z_1^2(k_sd) + Z_2^2(k_sd) - Z_1(k_sd)Z_3(k_sd)] + 2\int_d^a Z_0(k_sr)Z_2(k_sr)rdr\}$$

$$- 2\frac{C_{1s}D_{1s}}{\hat{z}_{II}} k_s^2 \frac{\ell\pi}{L} \int_d^a [Z_0(k_sr)\{X_0(k_sr) - X_2(k_sr)\} + Z_2(k_sr)$$

$$\{X_0(k_sr) - X_2(k_sr)\}]rdr + \frac{D_{1s}^2}{\hat{z}_{II}^2} k_s^2 [\frac{\ell\pi}{L}]^2 \{\frac{a^2}{2} [X_1^2(k_sa)$$

$$- X_1(k_sa)X_3(k_sa)] - \frac{d^2}{2} [X_0^2(k_sd) + X_1^2(k_sd) + X_2^2(k_sd) - X_1(k_sd)X_3(k_sd)]$$

$$- 2\int_d^a X_0(k_sr)X_2(k_sr)rdr\}]$$

$$+ \frac{\pi}{4} \sum_{s=1}^{\infty} \sum_{\substack{u=1 \\ u\neq s}}^{\infty} [C_{1s}C_{1u}k_sk_u \{\frac{2d}{k_s^2-k_u^2} [k_uZ_1(k_ud)Z_1'(k_sd)$$

$$- k_sZ_1'(k_ud)Z_1(k_sd)] + \int_d^a [Z_0(k_sr)Z_2(k_ur) + Z_2(k_sr)Z_0(k_ur)]rdr\}$$

$$+ 2\frac{C_{1s}D_{1u}}{\hat{z}_{II}} k_sk_u \frac{\ell\pi}{L} \{\frac{a}{k_s^2-k_u^2} [k_uZ_0(k_sa)X_1(k_ua) - k_uZ_2(k_sa)X_1(k_ua)]$$

$$+ \frac{2d}{k_s^2-k_u^2} [k_sZ_1(k_sd)X_1'(k_ud) - k_uZ_1'(k_sd)X_1(k_ud)]$$

$$+ \int_d^a [Z_0(k_sr)X_2(k_ur) - Z_2(k_sr)X_0(k_ur)]rdr\}$$

$$- \frac{D_{1s}D_{1u}}{\hat{z}_{II}^2} k_sk_u [\frac{\ell\pi}{L}]^2 \{\frac{2d}{k_s^2-k_u^2} [k_sX_1(k_sd)X_1'(k_ud) - k_uX_1'(k_sd)X_1(k_ud)]$$

$$- \int_d^a [X_0(k_sr)X_2(k_ur) + X_2(k_sr)X_0(k_ur)]rdr\}]$$

$$I_8 = \frac{\pi}{4} \sum_{s=1}^{\infty} [C_{1s}^2k_s^2 \{\frac{a^2}{2} [Z_0^2(k_sa) + Z_2^2(k_sa)] - \frac{d^2}{2} [Z_0^2(k_sd)$$

$$+ Z_1^2(k_sd)+Z_2^2(k_sd)-Z_1(k_sd)Z_3(k_sd)] - 2\int_d^a Z_0(k_sr)Z_2(k_sr)rdr\}$$

$$- 2\frac{C_{1s}D_{1s}}{\hat{z}_{II}} k_s^2 \frac{\ell\pi}{L} \int_d^a [Z_0(k_sr)\ \{X_0(k_sr) + X_2(k_sr)\} - Z_2(k_sr)$$

$$\{X_0(k_sr)+X_2(k_sr)\}]rdr + \frac{D_{1s}^2}{\hat{z}_{II}^2} k_s^2 [\frac{\ell\pi}{L}]^2\{\frac{a^2}{2} [X_0^2(k_sa)$$

$$+ X_2^2(k_sa)] - \frac{d^2}{2} [X_0^2(k_sd)+X_1^2(k_sd)+X_2^2(k_sd)-X_1(k_sd)X_3(k_sd)]$$

$$+ 2\int_d^a X_0(k_sr)X_2(k_sr)rdr\}]$$

$$+ \frac{\pi}{4}\sum_{s=1}^{\infty}\sum_{\substack{u=1\\u\neq s}}^{\infty} [C_{1s}C_{1u}k_sk_u \{\frac{2d}{k_s^2-k_u^2} [k_sZ_1(k_sd)Z_1'(k_ud)$$

$$- k_uZ_1'(k_sd)Z_1(k_ud)] + \int_d^a [Z_0(k_sr)Z_2(k_ur)+Z_2(k_sr)Z_0(k_ur)]rdr$$

$$+ 2\frac{C_{1s}D_{1u}}{\hat{z}_{II}} k_sk_u \frac{\ell\pi}{L} \{\frac{a}{k_s^2-k_u^2} [k_uX_1(k_ua)\{Z_0(k_sa)+Z_2(k_sa)\}]$$

$$+ \frac{d}{k_s^2-k_u^2} [k_sZ_1(k_sd)\{X_0(k_ud)+X_2(k_ud)\} - k_uX_1(k_ud)\{Z_0(k_sd)+Z_2(k_sd)\}]$$

$$+ \int_d^a [Z_0(k_sr)X_2(k_ur) - Z_2(k_sr)X_0(k_ur)]rdr$$

$$+ \frac{D_{1s}D_{1u}}{\hat{z}_{II}^2} k_sk_u [\frac{\ell\pi}{L}]^2 \{\frac{2d}{k_s^2-k_u^2} [k_uX_1(k_ud)X_1'(k_sd)$$

$$- k_sX_1(k_sd)X_1'(k_ud)] + \int_d^a [X_0(k_sr)X_2(k_ur) + X_2(k_sr)X_0(k_ur)]rdr\}]$$

$$I_9 = \frac{\pi L}{2}\sum_{s=1}^{\infty} \frac{D_{1s}}{\hat{z}_{II}^2} k_s^4 X_1^2(k_sa)$$

$$+ \frac{\pi L}{2} \sum_{s=1}^{\infty} \sum_{\substack{u=1 \\ u \neq s}}^{\infty} \frac{D_{1s} D_{1u}}{\hat{z}_{II}^2} k_s^2 k_u^2 \; X_1(k_s a) X_1(k_u a)$$

$$I_{10} = \frac{\pi L}{2} \sum_{s=1}^{\infty} [C_{1s}^2 k_s^2 \; Z_1'^2(k_s a) - 2\frac{C_{1s} D_{1s}}{\hat{z}_{II}} \; k_s \frac{\ell\pi}{L} Z_1'(k_s a) X_1(k_s a)$$

$$+ \frac{D_{1s}^2}{\hat{z}_{II}^2} \; [\frac{\ell\pi}{aL}]^2 \; X_1^2(k_s a)]$$

$$+ \frac{\pi L}{2} \sum_{s=1}^{\infty} \sum_{\substack{u=1 \\ u \neq s}}^{\infty} [C_{1s} C_{1u} k_s k_u \; Z_1'(k_s a) Z_1'(k_u a) - 2\frac{C_{1s} D_{1u}}{\hat{z}_{II}} k_s \frac{\ell\pi}{L} Z_1'(k_s a) X_1(k_u a)$$

$$+ \frac{D_{1s} D_{1u}}{\hat{z}_{II}^2} \; [\frac{\ell\pi}{a\ell}]^2 \; X_1(k_s a) X_1(k_u a)]$$

where

$$F_1(q,u) = \frac{\alpha_u \sin\alpha_q L \cos\alpha_u L - \alpha_q \cos\alpha_q L \sin\alpha_u L}{\alpha_q^2 - \alpha_u^2}$$

$$F_2(q,u) = \frac{\alpha_q \sin\alpha_q L \cos\alpha_u L - \alpha_u \cos\alpha_q L \sin\alpha_u L}{\alpha_q^2 - \alpha_u^2}$$

$$T(q,u) = \frac{\alpha_q - \alpha_q \cos\alpha_q L \cos\alpha_u L - \alpha_u \sin\alpha_q L \sin\alpha_u L}{\alpha_q^2 - \alpha_u^2}$$

$$Z_m(x) = J_m(x) + R_m^M \, N_m(x)$$

$$X_m(x) = J_m(x) + R_m^E \, N_m(x)$$

and the remaining integrals must be done numerically.

REFERENCES

(1) R.O. Bolt and J.G. Carroll, Radiation Effects on Organic Materials, New York, Academic Press, 1963, pp 325-334

(2) L. Solymar, Step Transducer Between Over-Moded Circular Waveguides, Proc. IEE Convention on Long Distance Transmission by Waveguide Part B Supplement pp 129-131, Jan. 1959

(3) L.R. Yavich, The Input Impedance of Stepped Convertors, Radiotechnika (USSR), Vol. 17, pp 22-25, March 1962

(4) L. Young, Stepped-Impedance Transformers and Filter Prototypes IRE Trans. Microwave Theory Tech., Vol. MTT-10, pp 339-359, Sept. 1962

(5) D.C. Thorn and A.W. Straiton, Design of Open-Ended Microwave Resonant Cavities, IRE Trans. Microwave Theory Techn., Vol. MTT-7, pp 389-390, July 1959

(6) N.C. Wenger and J. Smetana, Hydrogen Density Measurements Using Open-Ended Microwave Cavity, IEEE Trans. Instrum. Meas., Vol. IM-21, pp 105-144, May 1972

(7) G.S.P. Castle and J. Roberts, A Microwave Instrument for Continuous Monitoring of the Water Content of Crude Oil, Proc. IEEE, Vol. 62, pp 103-108, Jan. 1974

(8) S.S. Stuchly , M.A. Rzepecka and M.A.K. Hamid, A Microwave Open-Ended Cavity as a Void Fraction Monitor for Organic Coolants, IEEE Trans. Ind. Elec. Cont. Instrum., Vol. IECI-21, pp 78-80, May 1974

(9) W.C. Hahn, A New Method for the Calculation of Cavity Resonators, J. App. Phys., Vol. 12, pp62-68, Jan. 1941

(10) D.M. Bolle, Eigenvalue for a Centrally Loaded Circular Cylindrical Cavity, IRE Trans. Microwave Theory Tech., Vol. MTT-10, p 132, March 1962

(11) P. Bhartia and M.A.K. Hamid, Field Distribution in a Centrally Loaded Circular Cavity, IEEE Trans. on Nuclear Science, Vol. NS-16, pp 27-34, April 1969

(12) J.A. Stratton, "Electromagnetic Theory", New York: McGraw-Hill, pp 205-215, 1944

(13) C.J.F. Bottcher, "Theory of Electrical Polarization", Amsterdam, The Netherlands: Elsevier, pp 417-419, 1952

(14) L. Lewin, The Electrical Constants of a Material Loaded with Spherical Particles, Proc. IEE, Vol. 94, pt. III, p 65, 1947

(15) D.A.G. Bruggeman, Ann. Phys. ser 5, Vol. 24, p 636, 1935

(16) R. F. Harrington, "Time Harmonic Electromagnetic Fields", New York: McGraw-Hill, 1961, pp 219-222

(17) J. Van Bladel, "Electromagnetic Fields", New York: McGraw-Hill, 1964, p 448

(18) R.F. Harrington, "Time Harmonic Electromagnetic Fields", New York: McGraw-Hill, 1961, pp 73-76

(19) A.A. Oliner, A New Class of Reactive-Wall Waveguides for Low-Loss Applications, URSI General Assembly, Ottawa, Canada, Aug. 18-28, 1969

(20) S.J. Towaij and M.A.K. Hamid, Radiation by a Dielectric Loaded Cylindrical Antenna with a Wall Air Gap, Proc. IEE, Vol. 119, No. 1, pp 48-54, Jan. 1972

(21) J.H. Boyachok and M.A.K. Hamid, Analysis of a Microwave Void Fraction Meter, IEEE Trans. Ind. Elec. Cont. Instrum., Accepted for publication in 1974.